that TGF-β1 alone is not sufficient to induce an invasive phenotype in MCF10A cells.

3.4. ZEB1 knockdown in RARA-expressing MCF10A cells inhibited EMT and protrusion

To further investigate the mechanism of EMT induced by RARA, we established MCF10A cells that express RARA under the control of a tetracycline-responsive DNA element. We examined the effects of silencing of ZEB1 and ZEB2 using short hairpin RNAs (shRNAs) in the cells because these genes exhibited the most marked increase in expression levels among the known key EMT-inducing transcription factors (Figure 3C). We obtained two shRNAs (Figure 4A) and one shRNA (Figure 4B) that efficiently suppressed ZEB1 and ZEB2 mRNAs induced by RARA, respectively. Western blot analysis of EMT markers revealed that reduction of ZEB1 inhibited RARA-induced EMT, whereas that of ZEB2 did not (Figure 4C). Furthermore, we observed ZEB1 knockdown inhibited the protrusive phenotype in Matrigel and collagen I cultures caused by RARA (Figure 4D). These results indicate that ZEB1 is required for the RARA-mediated EMT and invasive phenotype.

4. Discussion

ERBB2 amplification is a so-called "driver" mutation (Stratton et al., 2009) that confers growth advantages on cancer cells. However, accumulating evidence suggests that breast cancer development probably results from the involvement of some other genes coamplified with ERBB2 in the 17q12–21 amplicon, not through ERBB2 acting alone. For example, previous studies identified that STARD3 and C35 localized within the amplicon expressed with ERBB2, and contributed to upregulated proliferation, decreased cell death, cell cycle progression (Kao and Pollack, 2006), and malignancy of breast cancer cells (Katz et al., 2010). We recently reported that GRB7, which is also located in the 17q12–21 amplicon, transforms NIH3T3 cells due to enhancement of ERBB2-mediated signaling pathways (Saito et al., 2012). In this report, we examined the genes in the amplicon for their ability to transform 3D-cultured MCF10A, and identified RARA, which disrupted acinar structures (Figure 1C) and induced EMT (Figure 3A and B). In contrast to the synergetic transforming activity of ERBB2 and GRB7 (Saito et al., 2012), RARA independently induced an invasive phenotype (Figure 2A). These studies indicate that the 17q12–21 amplicon harbors a surprising number of genes that play functional roles in the development and progression of breast cancers.

RARA amplification in parallel with ERBB2 in breast tumors was first reported by Keith et al. (1993) and is observed in 26.7% of ERBB2-amplified breast cancer patients. Such simultaneous amplification is statistically associated with malignant lesions, such as lymph node invasion (Lamy et al., 2011), suggesting that RARA could have the potential to efficiently promote progression to malignancy. Furthermore, Peng et al. (2004) described that RARα expression was enhanced in premalignant MCF10AT and malignant MCF10CA1a cells at the protein level, and suggested the association between upregulation of RARα and malignant transformation of MCF10A cells.

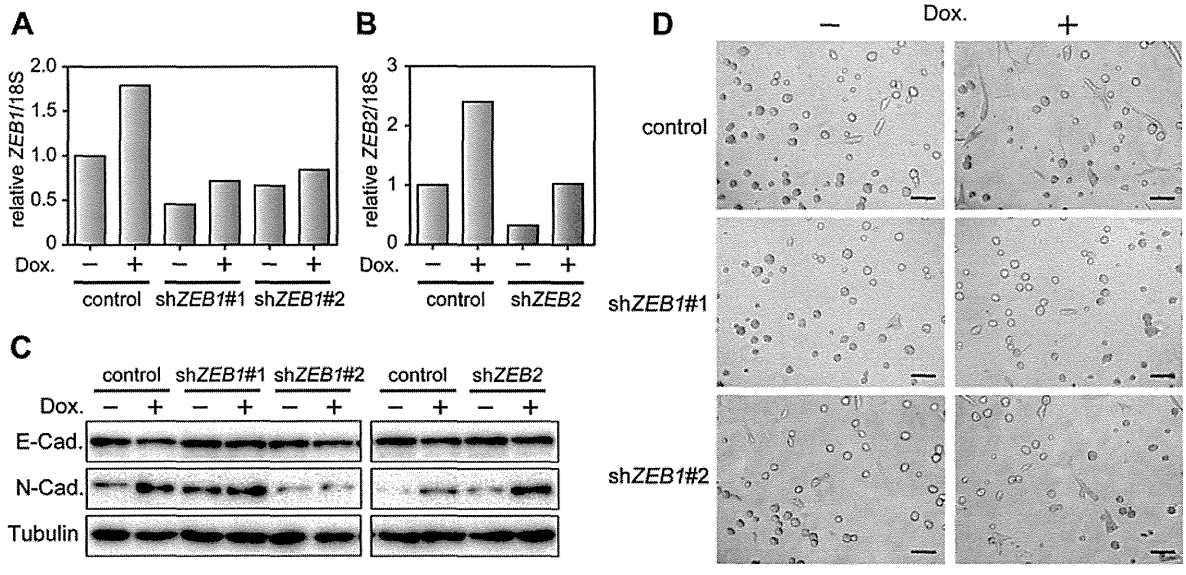

Figure 4 – Essential roles of ZEB1 in *RARA*-induced invasive phenotype. (A, B) Assessment of knockdown effects of shRNAs targeting *ZEB1* and *ZEB2*. MCF10A/Tet-on/TRE-*RARA* cells infected with indicated shRNA viral vectors were cultured in the absence or presence of Dox for 3 days. *ZEB1* and *ZEB2* mRNA was analyzed by real-time PCR analysis. The data were normalized by the amount of 18S rRNA and shown as a relative value compared with the control shRNA-infected cells without Dox. Representative results of one of two independent experiments are shown. (C) Inhibition of *RARA*-induced typical EMT marker transition by *ZEB1* knockdown. Protein extracts from the *ZEB1*- or *ZEB2*-knockdown cells were analyzed by immunoblotting. These cells were prepared as shown in (A) and (B), and cultured in Dox for 4 days with one passage. Tubulin was used as a loading control. (D) Inhibition of an *RARA*-induced protrusive phenotype in Matrigel and collagen I cultures by *ZEB1* knockdown. The *ZEB1*-knockdown cells were prepared as shown in (A), and cultured in Dox for 2 days in 2D cultures and for 4 additional days in 3D cultures. Invasive protrusions of these cells in Matrigel and collagen I cultures were observed on day 4.

Our results that *RARA* overexpression contributes to the phenotypic change of non-malignant cells to invasiveness support these hypotheses for the first time. We propose that *RARA* expression levels could be an important indicator to evaluate breast cancer malignancy.

Classically, RAR family members form heterodimers with retinoid X receptor (RXR) family members. Their ligand, retinoic acid (RA), activates these heterodimers, consequently leading to differentiation, apoptosis, and cell cycle arrest through transcriptional activation (Bastien and Rochette-Egly, 2004; Altucci and Gronemeyer, 2001). Consistent with these observations, a recent study revealed that *ERBB2*$^{+}$/*RARA*$^{+}$ breast cancer cells undergo apoptosis by the combination of a specific ERBB2 inhibitor, trastuzumab and a pan-RAR ligand, all-trans retinoic acid (ATRA) (Paroni et al., 2012). Here we demonstrated that overexpression of RARα accompanied by transcriptional activation induced large acinar structures presumably filled with surviving inner cells (Figure 1C and S3A). These results are apparently opposed to the effect of ATRA. It is known that ATRA differentially regulates all α, β and γ members of RARs. A previous report has shown that ATRA suppresses RARα expression in premalignant MCF10AT and malignant MCF10CA1a cells, while it suppresses RARγ expression only in MCF10CA1a cells (Peng et al., 2004). Also, it is known that distinct RXR-RAR isotype combinations lead to different expression patterns of RA-responsive genes (Chiba et al., 1997). Thus, we assume that the individual role of each RAR subtype is different and that phenotypes of breast cancer cells caused by treatment with ATRA represent effects on not only RARα but also RARβ and γ. Further analyses are needed to contribute to the understanding of the whole regulatory role of RARs.

In addition to typical heterodimer formation, another mechanism of RARα-induced cell-fate decisions could be considered. Previous studies implicated that RARα is an essential component of the estrogen receptor (ER) transcription complex and regulates the expression of estrogen-target genes, leading to cell proliferation in ER-positive cell lines (Ross-Innes et al., 2010; Toma et al., 1998). Activation of the classical RARα pathways could deplete RARα from the ER complex (Ross-Innes et al., 2010). Thus, any shift between the classical and non-classical RARα-pathways is assumed to influence cell fate. Previous evidence showed that intracellular lipid binding proteins, CRABP-II and FABP5, delivered RA from the cytosol to each particular nuclear receptor RARα and PPARβ/γ, respectively (Schug et al., 2007). It can be considered that dominant expression of FABP5 abolishes CRABP-II-mediated import of RA to RARα-RXR heterodimers, activating the non-classical pathway, while that of CRABP-II stimulates the classical pathway. Thus, the relative expression levels between those intracellular lipid binding proteins might be important to determine which classical or non-classical pathway RARα preferentially contributes to. Taken together, whether RARα promotes or suppresses tumor progression relies on several cellular contexts including the expression levels of ligands, nuclear hormone receptors and intracellular lipid-binding proteins. Efforts to identify RARα interaction targets in MCF10A cells will provide a molecular basis for the positive transforming activity observed in this study.

We observed that overexpression of *RARA* in MCF10A cells induced EMT (Figure 3A and B). The mechanisms inducing EMT are quite complex because a variety of signal transduction cascades such as the TGF-β, Wnt, Notch, EGF, FGF, and HIF pathways are involved (Polyak and Weinberg, 2009; Yang and Weinberg, 2008; Thiery et al., 2009). Which pathway is employed is dependent on the tissue, and even in the same tissue, on the particular cellular context. Our study suggests that MCF10A cells utilize, in part, the TGF-β pathway in the context of *RARA* overexpression (Figure S5). Repression of E-cadherin is an established hallmark of EMT, which is directly or indirectly mediated by EMT-inducing transcription factors including SNAIL, TWIST, SLUG, ZEB1, and ZEB2 (reviewed in Polyak and Weinberg (2009); Yang and Weinberg (2008); Thiery et al. (2009)). There is also extensive crosstalk among the factors that make up the "EMT interactome". In this network, a single EMT-inducing transcription factor affects the expression of other EMT-inducing transcription factors (Taube et al., 2010). It is likely that the EMT-interactome in mammary epithelial MCF10A cell lines is activated within 24 h after induction of *RARA* expression, as shown in Figure S4. During this period, RARα may activate the transcription of several EMT-related genes and subsequently regulate other EMT inducers, coordinately contributing to execution of the EMT program. Our results that *ZEB1*-depleted cells did not induce EMT phenotypes (Figure 4) strongly suggest that ZEB1 is a key factor for the RARα-activated EMT interactome. We also found that *RARA* overexpression upregulates *TGFB2* (Figure 3C), raising the possibility that RARα is involved in autocrine TGF-β/ZEB/miR-200 signaling (Burk et al., 2008; Gregory et al., 2011).

Accumulating evidence suggests that cells undergoing EMT acquire stem cell-like properties (Mani et al., 2008). RARα may also contribute to these changes. A recent report showed that mammary epithelium obtained from RARα1 knockout mice contained a greater percentage of progenitors but fewer mammary stem cells (MaSCs) compared with wild type, suggesting that RARα plays an important role in the maintenance of MaSCs, and affects the mammary epithelial hierarchy (Cohn et al., 2010). Furthermore, another report has shown that ZEB1 is required for the initial acquisition of both CD44^{hi} expression, which is a marker of breast cancer stem cells (BCSCs), and the stem-like activity of CD44^{hi} cells (Chaffer et al., 2013). In pancreatic cancer cells, ZEB1 maintains stem-like properties via downregulation of miR-183, 200c, and 203, which suppress the expression of stem cell factors such as BMI1, SOX2, and KLF4 (Wellner et al., 2009). Future experiments are required to investigate the potential role of the RARα–ZEB1 axis as a promoting factor of MaSCs and BCSCs.

5. Conclusion

We established an MCF10A 3D culture-based screening system and performed a screen of genes coamplified with *ERBB2* in the 17q12–21 amplicon. As a result, we revealed that *RARA* induced the malformation of acinar structures in Matrigel and facilitated an invasive phenotype in Matrigel/collagen I 3D culture. Furthermore, *RARA* upregulated the

transcription of EMT-related genes including ZEB1, which was a key mediator of EMT in RARA-expressing MCF10A cells. Our results suggest that overexpression of RARA is a potentially important factor for breast cancer malignancy.

Conflict of interest

The authors declare no conflict of interest.

Acknowledgments

We would like to acknowledge the secretarial assistance of Kumiko Semba. This research was partially supported by Japan Society for the Promotion of Science KAKENHI 23241064 and a grant for Translational Research Program: Achievement of personalized medicine and acceleration of anti-cancer drug development by using gene expression analysis technology from the New Energy and Industrial Technology Development Organization (NEDO).

Appendix A. Supplementary data

Supplementary data related to this article can be found at http://dx.doi.org/10.1016/j.molonc.2014.09.005.

REFERENCES

Altucci, L., Gronemeyer, H., 2001. The promise of retinoids to fight against cancer. Nat. Rev. Cancer 1, 181–193.

Baselga, J., Swain, S.M., 2009. Novel anticancer targets: revisiting ERBB2 and discovering ERBB3. Nat. Rev. Cancer 9, 463–475.

Bastien, J., Rochette-Egly, C., 2004. Nuclear retinoid receptors and the transcription of retinoid-target genes. Gene 328, 1–16.

Bieche, I., Tomasetto, C., Regnier, C.H., Moog-Lutz, C., Rio, M.C., Lidereau, R., 1996. Two distinct amplified regions at 17q11-q21 involved in human primary breast cancer. Cancer Res. 56, 3886–3890.

Burk, U., Schubert, J., Wellner, U., Schmalhofer, O., Vincan, E., Spaderna, S., Brabletz, T., 2008. A reciprocal repression between ZEB1 and members of the miR-200 family promotes EMT and invasion in cancer cells. EMBO Rep. 9, 582–589.

Chaffer, C.L., Marjanovic, N.D., Lee, T., Bell, G., Kleer, C.G., Reinhardt, F., D'Alessio, A.C., Young, R.A., Weinberg, R.A., 2013. Poised chromatin at the ZEB1 promoter enables breast cancer cell plasticity and enhances tumorigenicity. Cell 154, 61–74.

Chiba, H., Clifford, J., Metzger, D., Chambon, P., 1997. Distinct retinoid X receptor-retinoic acid receptor heterodimers are differentially involved in the control of expression of retinoid target genes in F9 embryonal carcinoma cells. Mol. Cell. Biol. 17, 3013–3020.

Chomczynski, P., Sacchi, N., 1987. Single-step method of RNA isolation by acid guanidinium thiocyanate-phenol-chloroform extraction. Anal. Biochem. 162, 156–159.

Cohn, E., Ossowski, L., Bertran, S., Marzan, C., Farias, E.F., 2010. RARalpha1 control of mammary gland ductal morphogenesis and wnt1-tumorigenesis. Breast Cancer Res. 12, R79.

Debnath, J., Brugge, J.S., 2005. Modelling glandular epithelial cancers in three-dimensional cultures. Nat. Rev. Cancer 5, 675–688.

Debnath, J., Muthuswamy, S.K., Brugge, J.S., 2003. Morphogenesis and oncogenesis of MCF-10A mammary epithelial acini grown in three-dimensional basement membrane cultures. Methods 30, 256–268.

Espina, V., Liotta, L.A., 2011. What is the malignant nature of human ductal carcinoma in situ? Nat. Rev. Cancer 11, 68–75.

Farboud, B., Hauksdottir, H., Wu, Y., Privalsky, M.L., 2003. Isotype-restricted corepressor recruitment: a constitutively closed helix 12 conformation in retinoic acid receptors beta and gamma interferes with corepressor recruitment and prevents transcriptional repression. Mol. Cell. Biol. 23, 2844–2858.

Gregory, P.A., Bracken, C.P., Smith, E., Bert, A.G., Wright, J.A., Roslan, S., Morris, M., Wyatt, L., Farshid, G., Lim, Y.Y., Lindeman, G.J., Shannon, M.F., Drew, P.A., Khew-Goodall, Y., Goodall, G.J., 2011. An autocrine TGF-beta/ZEB/miR-200 signaling network regulates establishment and maintenance of epithelial-mesenchymal transition. Mol. Biol. Cell 22, 1686–1698.

Jacot, W., Fiche, M., Zaman, K., Wolfer, A., Lamy, P.J., 2013. The HER2 amplicon in breast cancer: topoisomerase IIA and beyond. Biochim. Biophys. Acta 1836, 146–157.

Kao, J., Pollack, J.R., 2006. RNA interference-based functional dissection of the 17q12 amplicon in breast cancer reveals contribution of coamplified genes. Genes Chromosomes Cancer 45, 761–769.

Katz, E., Dubois-Marshall, S., Sims, A.H., Faratian, D., Li, J., Smith, E.S., Quinn, J.A., Edward, M., Meehan, R.R., Evans, E.E., Langdon, S.P., Harrison, D.J., 2010. A gene on the HER2 amplicon, C35, is an oncogene in breast cancer whose actions are prevented by inhibition of Syk. Br. J. Cancer 103, 401–410.

Kauraniemi, P., Barlund, M., Monni, O., Kallioniemi, A., 2001. New amplified and highly expressed genes discovered in the ERBB2 amplicon in breast cancer by cDNA microarrays. Cancer Res. 61, 8235–8240.

Keith, W.N., Douglas, F., Wishart, G.C., McCallum, H.M., George, W.D., Kaye, S.B., Brown, R., 1993. Co-amplification of erbB2, topoisomerase II alpha and retinoic acid receptor alpha genes in breast cancer and allelic loss at topoisomerase I on chromosome 20. Eur. J. Cancer 29A, 1469–1475.

Kleinman, H.K., McGarvey, M.L., Liotta, L.A., Robey, P.G., Tryggvason, K., Martin, G.R., 1982. Isolation and characterization of type IV procollagen, laminin, and heparan sulfate proteoglycan from the EHS sarcoma. Biochemistry 21, 6188–6193.

Lamy, P.J., Fina, F., Bascoul-Mollevi, C., Laberenne, A.C., Martin, P.M., Ouafik, L., Jacot, W., 2011. Quantification and clinical relevance of gene amplification at chromosome 17q12-q21 in human epidermal growth factor receptor 2-amplified breast cancers. Breast Cancer Res. 13, R15.

Lu, J., Guo, H., Treekitkarnmongkol, W., Li, P., Zhang, J., Shi, B., Ling, C., Zhou, X., Chen, T., Chiao, P.J., Feng, X., Seewaldt, V.L., Muller, W.J., Sahin, A., Hung, M.C., Yu, D., 2009. 14-3-3zeta Cooperates with ErbB2 to promote ductal carcinoma in situ progression to invasive breast cancer by inducing epithelial-mesenchymal transition. Cancer Cell 16, 195–207.

Mani, S.A., Guo, W., Liao, M.J., Eaton, E.N., Ayyanan, A., Zhou, A.Y., Brooks, M., Reinhard, F., Zhang, C.C., Shipitsin, M., Campbell, L.L., Polyak, K., Brisken, C., Yang, J., Weinberg, R.A., 2008. The epithelial-mesenchymal transition generates cells with properties of stem cells. Cell 133, 704–715.

Muthuswamy, S.K., Li, D., Lelievre, S., Bissell, M.J., Brugge, J.S., 2001. ErbB2, but not ErbB1, reinitiates proliferation and induces luminal repopulation in epithelial acini. Nat. Cell Biol. 3, 785–792.

Paroni, G., Fratelli, M., Gardini, G., Bassano, C., Flora, M., Zanetti, A., Guarnaccia, V., Ubezio, P., Centritto, F., Terao, M., Garattini, E., 2012. Synergistic antitumor activity of lapatinib and retinoids on a novel subtype of breast cancer with coamplification of ERBB2 and RARA. Oncogene 31, 3431–3443.

Peng, X., Yun, D., Christov, K., 2004. Breast cancer progression in MCF10A series of cell lines is associated with alterations in retinoic acid and retinoid X receptors and with differential response to retinoids. Int. J. Oncol. 25, 961–971.

Polyak, K., Weinberg, R.A., 2009. Transitions between epithelial and mesenchymal states: acquisition of malignant and stem cell traits. Nat. Rev. Cancer 9, 265–273.

Ross-Innes, C.S., Stark, R., Holmes, K.A., Schmidt, D., Spyrou, C., Russell, R., Massie, C.E., Vowler, S.L., Eldridge, M., Carroll, J.S., 2010. Cooperative interaction between retinoic acid receptor-alpha and estrogen receptor in breast cancer. Genes Dev. 24, 171–182.

Saito, M., Kato, Y., Ito, E., Fujimoto, J., Ishikawa, K., Doi, A., Kumazawa, K., Matsui, A., Takebe, S., Ishida, T., Azuma, S., Mochizuki, H., Kawamura, Y., Yanagisawa, Y., Honma, R., Imai, J., Ohbayashi, H., Goshima, N., Semba, K., Watanabe, S., 2012. Expression screening of 17q12-21 amplicon reveals GRB7 as an ERBB2-dependent oncogene. FEBS Lett. 586, 1708–1714.

Schug, T.T., Berry, D.C., Shaw, N.S., Travis, S.N., Noy, N., 2007. Opposing effects of retinoic acid on cell growth result from alternate activation of two different nuclear receptors. Cell 129, 723–733.

Seton-Rogers, S.E., Lu, Y., Hines, L.M., Koundinya, M., LaBaer, J., Muthuswamy, S.K., Brugge, J.S., 2004. Cooperation of the ErbB2 receptor and transforming growth factor beta in induction of migration and invasion in mammary epithelial cells. Proc. Natl. Acad. Sci. U S A 101, 1257–1262.

Stratton, M.R., Campbell, P.J., Futreal, P.A., 2009. The cancer genome. Nature 458, 719–724.

Taube, J.H., Herschkowitz, J.I., Komurov, K., Zhou, A.Y., Gupta, S., Yang, J., Hartwell, K., Onder, T.T., Gupta, P.B., Evans, K.W., Hollier, B.G., Ram, P.T., Lander, E.S., Rosen, J.M., Weinberg, R.A., Mani, S.A., 2010. Core epithelial-to-mesenchymal transition interactome gene-expression signature is associated with claudin-low and metaplastic breast cancer subtypes. Proc. Natl. Acad. Sci. U S A 107, 15449–15454.

Thiery, J.P., Acloque, H., Huang, R.Y., Nieto, M.A., 2009. Epithelial-mesenchymal transitions in development and disease. Cell 139, 871–890.

Toma, S., Isnardi, L., Raffo, P., Riccardi, L., Dastoli, G., Apfel, C., LeMotte, P., Bollag, W., 1998. RARalpha antagonist Ro 41-5253 inhibits proliferation and induces apoptosis in breast-cancer cell lines. Int. J. Cancer 78, 86–94.

Vargo-Gogola, T., Rosen, J.M., 2007. Modelling breast cancer: one size does not fit all. Nat. Rev. Cancer 7, 659–672.

Wellner, U., Schubert, J., Burk, U.C., Schmalhofer, O., Zhu, F., Sonntag, A., Waldvogel, B., Vannier, C., Darling, D., zur Hausen, A., Brunton, V.G., Morton, J., Sansom, O., Schuler, J., Stemmler, M.P., Herzberger, C., Hopt, U., Keck, T., Brabletz, S., Brabletz, T., 2009. The EMT-activator ZEB1 promotes tumorigenicity by repressing stemness-inhibiting microRNAs. Nat. Cell Biol. 11, 1487–1495.

Witt, A.E., Hines, L.M., Collins, N.L., Hu, Y., Gunawardane, R.N., Moreira, D., Raphael, J., Jepson, D., Koundinya, M., Rolfs, A., Taron, B., Isakoff, S.J., Brugge, J.S., LaBaer, J., 2006. Functional proteomics approach to investigate the biological activities of cDNAs implicated in breast cancer. J. Proteome Res. 5, 599–610.

Yamada, K.M., Cukierman, E., 2007. Modeling tissue morphogenesis and cancer in 3D. Cell 130, 601–610.

Yang, J., Weinberg, R.A., 2008. Epithelial-mesenchymal transition: at the crossroads of development and tumor metastasis. Dev. Cell 14, 818–829.

Yarden, Y., Sliwkowski, M.X., 2001. Untangling the ErbB signalling network. Nat. Rev. Mol. Cell Biol. 2, 127–137.

Article

TRANSPARENT PROCESS

THE EMBO JOURNAL

MiR-133 promotes cardiac reprogramming by directly repressing Snai1 and silencing fibroblast signatures

Naoto Muraoka[1,2], Hiroyuki Yamakawa[1,2], Kazutaka Miyamoto[1,2], Taketaro Sadahiro[1,2], Tomohiko Umei[1], Mari Isomi[1], Hanae Nakashima[1], Mizuha Akiyama[1], Rie Wada[1], Kohei Inagawa[1,2], Takahiko Nishiyama[1,2], Ruri Kaneda[1,2], Toru Fukuda[3], Shu Takeda[3], Shugo Tohyama[2], Hisayuki Hashimoto[2], Yoshifumi Kawamura[4], Naoki Goshima[5], Ryo Aeba[6], Hiroyuki Yamagishi[7], Keiichi Fukuda[2] & Masaki Ieda[1,2,8,*]

Abstract

Fibroblasts can be directly reprogrammed into cardiomyocyte-like cells (iCMs) by overexpression of cardiac transcription factors or microRNAs. However, induction of functional cardiomyocytes is inefficient, and molecular mechanisms of direct reprogramming remain undefined. Here, we demonstrate that addition of miR-133a (miR-133) to Gata4, Mef2c, and Tbx5 (GMT) or GMT plus Mesp1 and Myocd improved cardiac reprogramming from mouse or human fibroblasts by directly repressing Snai1, a master regulator of epithelial-to-mesenchymal transition. MiR-133 overexpression with GMT generated sevenfold more beating iCMs from mouse embryonic fibroblasts and shortened the duration to induce beating cells from 30 to 10 days, compared to GMT alone. Snai1 knockdown suppressed fibroblast genes, upregulated cardiac gene expression, and induced more contracting iCMs with GMT transduction, recapitulating the effects of miR-133 overexpression. In contrast, overexpression of Snai1 in GMT/miR-133-transduced cells maintained fibroblast signatures and inhibited generation of beating iCMs. MiR-133-mediated Snai1 repression was also critical for cardiac reprogramming in adult mouse and human cardiac fibroblasts. Thus, silencing fibroblast signatures, mediated by miR-133/Snai1, is a key molecular roadblock during cardiac reprogramming.

Keywords cardiomyocyte; microRNA; reprogramming; Snai1; transcription factor

Subject Categories Development & Differentiation; Stem Cells

DOI 10.15252/embj.201387605 | Received 16 December 2013 | Revised 18 April 2014 | Accepted 5 May 2014 | Published online 11 June 2014

The EMBO Journal (2014) 33: 1565–1581

Introduction

Direct reprogramming of mature cells from one lineage to another without passing through a stem cell state has emerged as a new strategy for generating cell types of interest and may hold great potential for regenerative medicine. Thus far, neurons, cardiomyocytes, hepatocytes, blood precursor cells, and neural progenitors were successfully induced from fibroblasts by overexpression of lineage-specific transcription factor (Ieda *et al*, 2010; Szabo *et al*, 2010; Vierbuchen *et al*, 2010; Sekiya & Suzuki, 2011; Han *et al*, 2012; Wada *et al*, 2013). Suppression of the starting-cell signature is a recognized characteristic of cell fate conversion, although the molecular mechanisms underlying this process and its importance during direct reprogramming remain poorly understood (Marro *et al*, 2011; Muraoka & Ieda, 2014).

It was reported that induced cardiomyocyte-like cells (iCMs) can be directly generated from mouse fibroblasts by the combination of transcription factors, Gata4, Mef2c, and Tbx5 (GMT), GMT plus Hand2 (GHMT), or Mef2c, Myocd, and Tbx5 *in vitro* (Ieda *et al*, 2010; Protze *et al*, 2012; Song *et al*, 2012). Recently, we and others reported that iCMs can be directly generated from human fibroblasts by overexpression of GMT plus Mesp1 and Myocd (GMTMM) or other combinations of reprogramming factors (Fu *et al*, 2013; Nam *et al*, 2013; Wada *et al*, 2013). However, induction of functional cardiomyocytes *in vitro* was inefficient and slow, possibly hindering our investigations of the molecular events during cardiac reprogramming (Chen *et al*, 2012; Srivastava & Ieda, 2012; Addis & Epstein, 2013). We and others also showed that endogenous mouse cardiac fibroblasts (CFs) can be converted into iCMs *in vivo* by gene transfer of GMT or GHMT (Inagawa *et al*, 2012; Qian *et al*, 2012;

1 Department of Clinical and Molecular Cardiovascular Research, Keio University School of Medicine, Shinjuku-ku, Tokyo, Japan
2 Department of Cardiology, Keio University School of Medicine, Shinjuku-ku, Tokyo, Japan
3 Department of Physiology and Cell Biology, Tokyo Medical and Dental University, Bunkyo-ku, Tokyo, Japan
4 Japan Biological Informatics Consortium (JBIC), Koto-ku, Tokyo, Japan
5 Molecular Profiling Research Center for Drug Discovery, National Institute of Advanced Industrial Science and Technology, Koto-ku, Tokyo, Japan
6 Division of Cardiovascular Surgery, Keio University School of Medicine, Shinjuku-ku, Tokyo, Japan
7 Department of Pediatrics, Keio University School of Medicine, Shinjuku-ku, Tokyo, Japan
8 JST, CREST, Shinjuku-ku, Tokyo, Japan
*Corresponding author. Tel: +81 3 5843 6702; Fax: +81 3 5363 3875; E-mail: mieda@z8.keio.jp

© 2014 The Authors

Song *et al*, 2012). The *in vivo* iCMs were more fully reprogrammed than their cultured counterparts, suggesting the presence of undefined factors that enhance reprogramming. Identification of such potent reprogramming factors could provide new insights into the mechanisms of cardiac reprogramming.

MicroRNAs (miRNAs) can suppress the expression of hundreds of genes, primarily through binding to the 3′-untranslated region (UTR) of target mRNAs, and thus play important roles in cell fate decisions. Embryonic stem cell-specific miRNAs enhanced the reprogramming efficiency of fibroblasts into induced pluripotent stem cells (iPSCs; Judson *et al*, 2009; Subramanyam *et al*, 2011), and more recently, Jayawardena *et al* (2012) reported that a combination of muscle-specific miRNAs (miR-1, 133, 208, 499) alone reprogrammed neonatal mouse CFs into cardiomyocyte-like cells (Jayawardena *et al*, 2012). However, it remains unclear whether other types of fibroblasts could also be converted into iCMs by miRNAs. Moreover, the global transcriptional changes and mechanistic basis of cardiac reprogramming by miRNAs remain unknown.

Here, we show that miR-133a (miR-133) promoted cardiac reprogramming in mouse embryonic fibroblasts (MEFs), adult mouse cardiac fibroblasts, and human cardiac fibroblasts (HCFs) in combination with GMT or GMTMM transduction. We found that miR-133 suppressed the fibroblast programs by directly repressing Snai1, a master regulator of epithelial-to-mesenchymal transition (EMT), and thereby promoted cardiac reprogramming.

Results

MiR-133 promotes cardiac induction in MEFs in combination with Gata4/Mef2c/Tbx5

We first investigated whether miR-1, 133, 208, and 499 alone, shown previously to induce cardiac reprogramming in neonatal mouse CFs, could also generate iCMs from MEFs, which have a distinct embryonic origin compared to CFs. We used MEFs from αMHC promoter-driven EGFP transgenic mice (αMHC-GFP), in which no cardiomyocytes or cardiac progenitor cells (CPCs) were detected by immunofluorescence, fluorescence-activated cell sorting (FACS), and quantitative RT-PCR (qRT-PCR) analyses (Supplementary Fig S1A–E; Ieda *et al*, 2010). The transfection efficiency by miRNA mimics was 97%, but none of the miRNA mimics induced αMHC-GFP or cardiac troponin T (cTnT) expression in MEFs when used individually or as a pool (four miRs) after 1 week of transfection (Fig 1A and B, Supplementary Fig S1F and G; Jayawardena *et al*, 2012). In contrast, GMT transduction induced αMHC-GFP and cTnT expression in MEFs, similar to that induced in CFs (Fig 1A and B, Supplementary Fig S1H; Ieda *et al*, 2010).

Next, we introduced these miRNAs along with GMT into MEFs to investigate whether miRNAs promote cardiac reprogramming. We found that the number of αMHC-GFP$^+$ cells activating a cardiac reporter was increased by approximately twofold and that the number of cTnT$^+$ cells expressing the endogenous cardiac-specific gene was increased by approximately sixfold by the addition of miR-1, 133, or four miRs to the GMT transduction (Fig 1C and D). In contrast, addition of miR-208 or miR-499 had no substantial effects, suggesting that the miRNA effects were specific. Among them, miR-133 mimics showed the greatest effects, and thereby, we used miR-133 in subsequent studies. We determined the dose dependency of miR-133-mediated cardiac induction and found that 15 nM of miR-133 was sufficient (Fig 1E and F). Addition of JAK inhibitor I, which reported to increase cardiac induction, to GMT/miR-133 did not augment the reprogramming efficiency (Supplementary Fig S1I and J; Jayawardena *et al*, 2012). FACS analyses demonstrated that expression of another cardiac marker, sarcomeric α-actinin (α-actinin), was also increased by addition of miR-133 to GMT (Fig 1G). Immunostaining for cardiac markers, including α-actinin, cTnT, and atrial natriuretic peptide (ANP), demonstrated that GMT/miR-133 strongly enhanced cardiac protein expression, and the iCMs had well-defined sarcomeric structures, similar to neonatal cardiomyocytes (Fig 1H and I, Supplementary Fig S1B). Thus, miR-133 improved cardiac induction from MEFs in combination with GMT transduction.

MiR-133 rapidly and efficiently induces functional cardiomyocyte-like cells from MEFs in combination with Gata4/Mef2c/Tbx5

To investigate the effects of miR-133 on cardiac reprogramming in more detail, we next compared the time courses of reprogramming between GMT and GMT/miR-133 induction. FACS analyses revealed that GMT/miR-133 induced significantly more α-MHC-GFP and cTnT expression in the MEFs by as early as day 3 than GMT alone, with the numbers peaking at day 7, and remaining higher even at 4 weeks after transduction (Fig 2A, Supplementary Fig S2A). The iCMs were less proliferative than non-converted fibroblasts and decreased in percentage relative to the total number of cells over time in culture. qRT-PCR demonstrated that the expression of cardiac genes, *Actn2* (sarcomeric α-actinin), *Myh6* (α-myosin heavy chain), *Ryr2* (ryanodine receptor 2), and *Tnni3* (cardiac troponin I), was upregulated, while the expression of fibroblast genes, *Col1a1* (collagen 1a1) and *Fn1* (fibronectin 1), was significantly downregulated from day 3 in the FACS-sorted α-MHC-GFP$^+$ cells

Figure 1. MiR-133 promotes Gata4/Mef2c/Tbx5-induced cardiac reprogramming.

A, B FACS analyses for αMHC-GFP$^+$ and cTnT$^+$ cells 1 week after GMT transduction or miRNA transfection. Quantitative data are shown in (B) (n = 3).

C, D FACS analyses for αMHC-GFP$^+$ and cTnT$^+$ cells 1 week after GMT and miRNA transduction. Quantitative data are shown in (D) (n = 3).

E, F Dose dependency of miR-133-mediated cardiac induction with GMT. Quantitative data are shown in (F) (n = 3).

G FACS analyses for α-actinin$^+$ cells 1 week after transduction.

H Immunocytochemisty for αMHC-GFP, α-actinin, and DAPI. GMT/miR-133 induced abundant αMHC-GFP and α-actinin expression 2 weeks after transduction. High-magnification views in insets show sarcomeric organization. GMT/miR-133 induced cTnT and ANP expression 2 weeks after transduction. Insets are high-magnification views.

Data information: All data are presented as means ± SEM. *P < 0.05, **P < 0.01 versus relevant control. Scale bars represent 100 μm.

 © 2014 The Authors

induced with GMT/miR-133 (Fig 2B). Non-sorted samples also revealed comparable results (Supplementary Fig S2B). Immunocytochemistry demonstrated that the GMT/miR-133-iCMs showed sarcomeric structures after 7 days of infection, which normally takes 2 weeks with GMT alone (Fig 2C). qRT-PCR and immunostaining for the genes specific to nodal, atrial, and ventricular myocytes

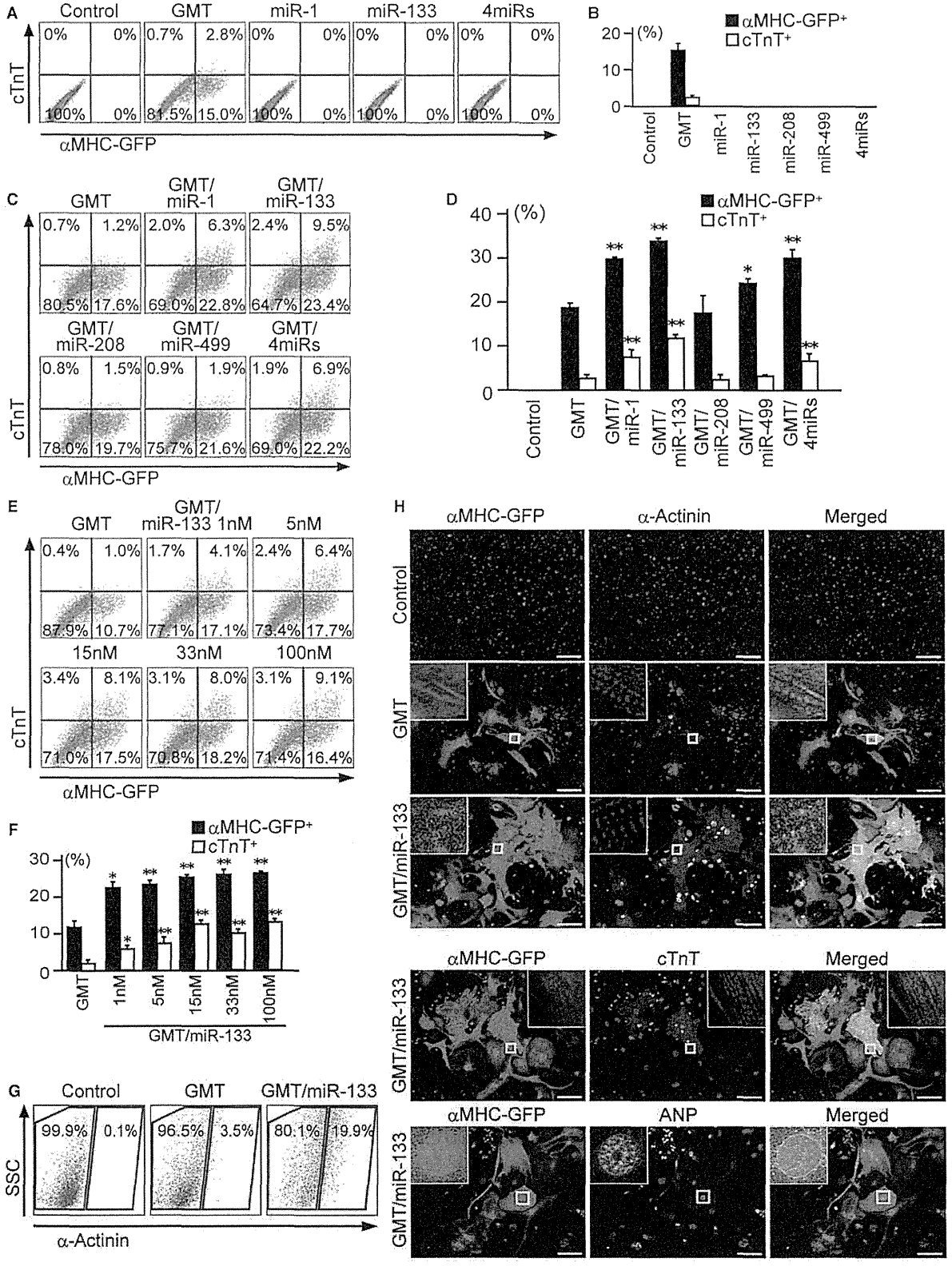

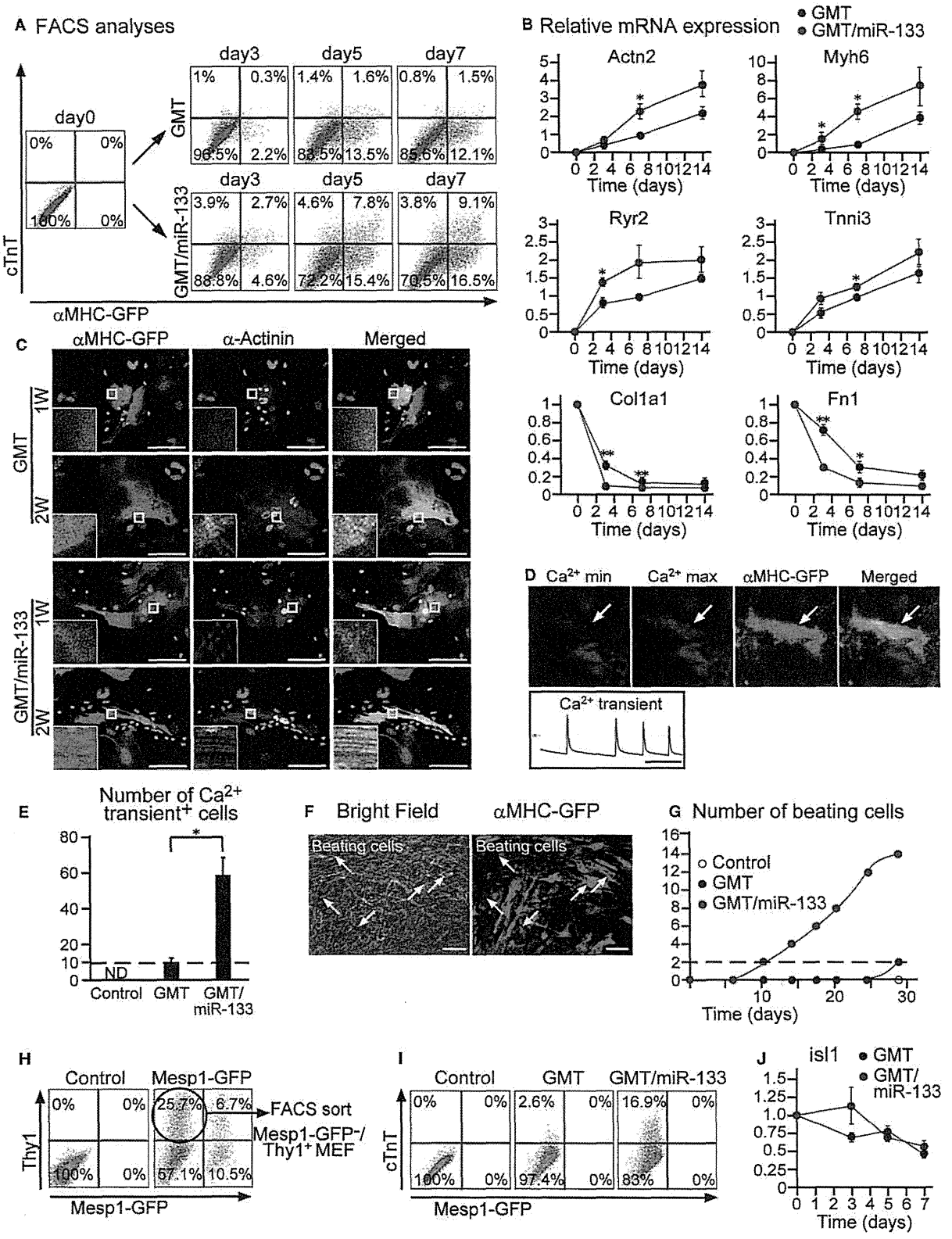

revealed that most iCMs were atrial-type myocytes with either transduction (Supplementary Fig S2C and D). Functionally, a subset of MEF-derived iCMs showed spontaneous Ca^{2+} oscillations, and sixfold more cells exhibited Ca^{2+} flux with GMT/miR-133 induction than with GMT alone (Fig 2D and E, Supplementary Movie S1). Notably, cell contraction started from 10 days after GMT/miR-133

© 2014 The Authors

Figure 2. MiR-133 enhances generation of functional iCMs.

A Time course of αMHC-GFP and cTnT expression by GMT or GMT/miR-133 transduction in MEFs. See also Supplementary Fig S2A.

B qRT-PCR for cardiac and fibroblast gene expression in αMHC-GFP$^+$ cells by GMT or GMT/miR-133 transduction (n = 4). Data were normalized against the values of GMT-iCMs at day 7 (*Actn2, Myh6, Ryr2, Tnni3*) or MEFs at day 0 (*Col1a1, Fn1*). See also Supplementary Fig S2B.

C GMT/miR-133 induced expression of α-actinin with sarcomeric organization 1 week after transduction.

D, E Spontaneous Ca^{2+} oscillations observed in MEF-derived iCMs (arrows) after 4 weeks of induction, corresponding to Supplementary Movie S1. Rhod-3 images at Ca^{2+} max and min are shown in the upper panels and Rhod-3 intensity trace is shown in the lower panel (D). Total number of Ca^{2+} oscillation$^+$ cells in 10 randomly selected fields per well is shown in (E) (n = 3).

F Spontaneously beating GMT/miR-133 iCMs 4 weeks after transduction (arrows), corresponding to Supplementary Movie S2. See also Supplementary Fig S2E and Movie S3.

G Number of spontaneously beating cells in each well after transduction of mock, GMT, or GMT/miR-133 at the indicated time.

H, I Mesp1-GFP$^-$/Thy1$^+$ MEFs were sorted and transduced with GMT or GMT/miR-133 (H). All cTnT$^+$ cells were negative for Mesp1-GFP (I).

J qRT-PCR for *isl1* expression in the cells transduced with GMT or GMT/miR-133 (n = 3).

Data information: All data are presented as means ± SEM. *P < 0.05, **P < 0.01 versus relevant control. Scale bars: 100 μm (C, F); 5 s (D).

transduction, which generally took 4 weeks with GMT. The number of beating cells increased over time, with sevenfold more contractile cells achieved compared to using GMT alone (Fig 2F and G, Supplementary Fig S2E, and Supplementary Movies S2 and S3). We did not observe any beating cells in untreated MEF cultures, excluding the possibility of cardiomyocyte contamination. EdU incorporation assays revealed that the increase in beating iCMs with GMT/miR-133 transduction was not due to cell proliferation (Supplementary Fig S2F and G). These results suggest that miR-133 promoted the speed and efficiency of cardiac reprogramming in combination with GMT.

Mesp1-GFP mice, in which the progeny of multipotent CPCs can be traced by fluorescence, were used to determine the route of cardiac reprogramming (Saga *et al*, 1999; Kawamoto *et al*, 2000). We isolated Mesp1-GFP$^-$/Thy1$^+$ MEFs by FACS and transduced the cells with GMT/miR-133 (Fig 2H). The resulting cTnT$^+$ cells did not express GFP, suggesting that the iCMs were generated from MEFs without passing through a mitotic Mesp1$^+$-CPC state (Fig 2I). Moreover, a later CPC marker, isl1, was not induced by GMT/miR-133 during reprogramming (Fig 2J). These results indicated that the iCMs were directly generated from fibroblasts by GMT/miR-133.

MiR-133 suppresses fibroblast signatures in concert with cardiac gene activation

Next, to investigate the mechanistic basis of miR-133-mediated cardiac reprogramming, we analyzed the global gene expression profiles of iCMs induced with GMT or GMT/miR-133 by microarray. We FACS-sorted α-MHC-GFP$^+$ cells at 3, 7, and 18 days after transduction, before and after the GMT/miR-133-transduced cells started contractions, and compared the differential gene expressions between MEFs and hearts. Although the vast majority of α-MHC-GFP$^+$ cells were only partially reprogrammed iCMs, with few capable of beating, the heatmap image of microarray data revealed a shift in the global gene expression patterns of the iCMs from a MEF state toward a cardiac-like phenotype by GMT or GMT/miR-133 transduction at all stages (Fig 3A). Next, to identify the genes that were regulated by miR-133, we focused on the genes that were differentially expressed between GMT and GMT/miR-133 transduction at all stages. Among 23,474 probes, 46 genes were upregulated, and 129 genes were downregulated by at least 1.5-fold by GMT/miR-133 induction, consistent with the function of miRNAs, typically diminishing the expression of their mRNA targets (Fig 3B, Supplementary Table S1). Gene ontology (GO) analyses demonstrated that upregulated genes in the GMT/miR-133-iCMs were significantly enriched for GO terms associated with cardiac function and development, while the downregulated genes were significantly enriched for the GO terms associated with fibroblast signatures, such as cell adhesion, cell proliferation, and collagen fibril organization (Fig 3C and D). Scatter plot analyses at day 3 of transduction demonstrated that the upregulated genes induced by GMT/miR-133 were significantly enriched in heart compared to MEFs (P = 7.7E-21), while the downregulated genes in GMT/miR-133-iCMs were highly enriched in MEFs (P = 1.2E-34), indicating that miR-133 induced cardiac gene programs and extinguished fibroblast signatures from the early stages of reprogramming (Fig 3E). Microarray and qRT-PCR analyses revealed that cardiac genes related to different functions, such as sarcomere structures (*Actn2, Myh6, Tnni3*), mitochondrial metabolism (*Ppargc1a*), and ion channels (*Ryr2, Slc8a1, Kcnd2,* and *Scn5a*), were upregulated, while fibroblast genes, *Snai1, Col1a1, Col1a2, Fn1,* and *Postn*, were downregulated in the GMT/miR-133-iCMs compared to the GMT-iCMs at day 7 (Fig 3F and G). Epithelial genes, such as *cdh1* (E-cadherin), *Dsp, Pkp1, Ctnnb1, F2r,* and *Ocln*, were not upregulated, suggesting miR-133 did not induce mesenchymal-to-epithelial transition (MET) process. Thus, miR-133 silenced fibroblast signatures in parallel with cardiac gene activation from the early stages of reprogramming.

MiR-133 directly represses Snai1 expression during cardiac reprogramming

We then searched for potential direct mRNA targets of miR-133 during cardiac reprogramming. Expression of *Ccnd2, Cdc42, Hand2, RhoA,* and *Srf*, shown previously as the direct targets of miR-133, was not significantly altered in GMT-miR-133-iCMs compared to GMT-iCMs, as shown by microarray (Fig 4A; Liu & Olson, 2010). Using the miRNA target prediction program, we identified Snai1 as a putative direct target of miR-133 with two conserved miR-133-binding sites within the 3′UTR (Fig 4B). Snai1 is a basic helix-loop-helix transcription factor, known as a master regulator of EMT, and induces mesenchymal programs and fibrogenesis during development and disease (Rowe *et al*, 2009; Li *et al*, 2010). In luciferase reporter assays with a construct containing a full-length Snai1 3′UTR sequence, miR-133 transfection strongly repressed the luciferase activity by 60%. Mutations of either predicted miR-133-binding site in the Snai1 3′UTR reduced the responsiveness to miR-133, which was almost absent with mutations of both sites, suggesting direct binding of miR-133 to both sites (Fig 4C). qRT-PCR confirmed that

© 2014 The Authors

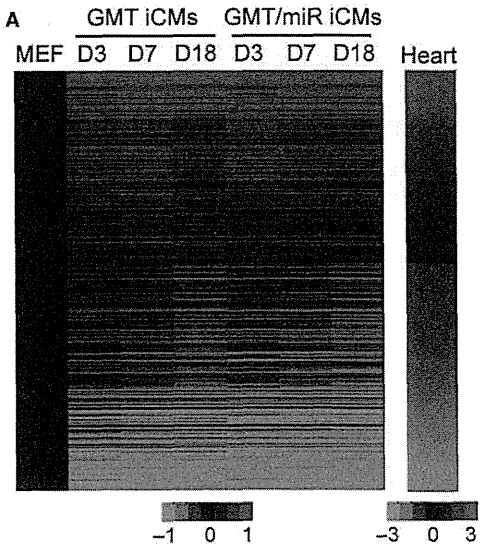

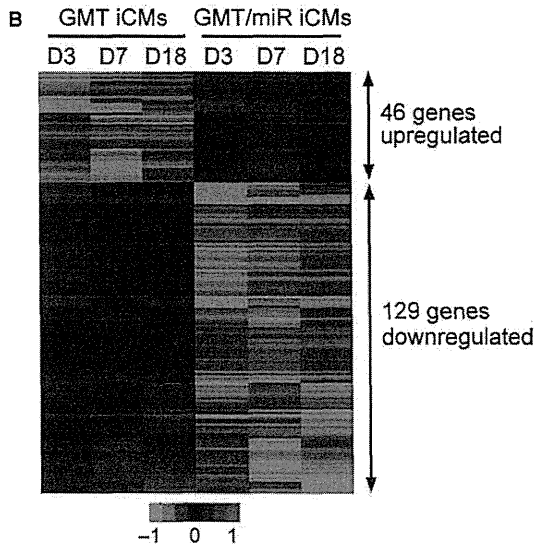

C GO categories enriched in GMT/miR iCMs upregulated genes

GO term	Genes	Size	p-value
Muscle contraction	4	47	1.2E-7
Muscle filament sliding	2	4	5.3E-6
Adult heart development	2	13	6.8E-5
Regulation of heart rate	2	13	6.8E-5
Focal adhesion assembly	2	15	9.2E-5
Cell chemotaxis	2	16	1.0E-4
ATP catabolic process	3	104	1.3E-4
Cardiac muscle morphogenesis	2	25	2.6E-4
cAMP metabolic process	1	1	9.5E-4
Visceral muscle development	1	1	9.5E-4

D GO categories enriched in GMT/miR iCMs downregulated genes

GO term	Genes	Size	p-value
Cell adhesion	11	455	1.1E-7
Regulation of cell prolifeartion	9	322	4.9E-7
Collagen fibril organization	4	27	1.2E-6
Protein heterotrimerization	3	8	1.4E-6
Positive regulation of apoptosis	7	199	2.1E-6
Cellular response to calcium ion	3	10	2.9E-6
Prostate gland morphogenesis	3	11	4.0E-6
Cellular response to amino acid	5	85	5.4E-6
Regulation of transcription	9	455	8.3E-6
Regulation of smooth muscle cell	4	48	1.2E-5

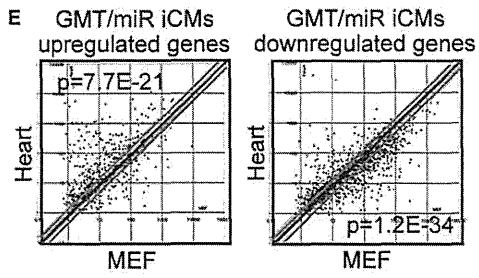

F Expression ratio (GMT/miR iCMs vs GMT iCMs)

Cardiac genes		Fibroblast genes		Epithelial genes	
Actn2	2.3	Snai1	0.6	Cdh1	1.1
Myh6	2.8	Snai2	0.7	Dsp	1.0
Tnni3	1.5	Col1a1	0.5	Pkp1	0.5
Ppargc1a	2.7	Col1a2	0.3	Ctnnb1	0.9
Slc8a1	2.0	Postn	0.4	F2r	0.7
Kcnd2	1.6	Fn1	0.5	Ocln	0.8

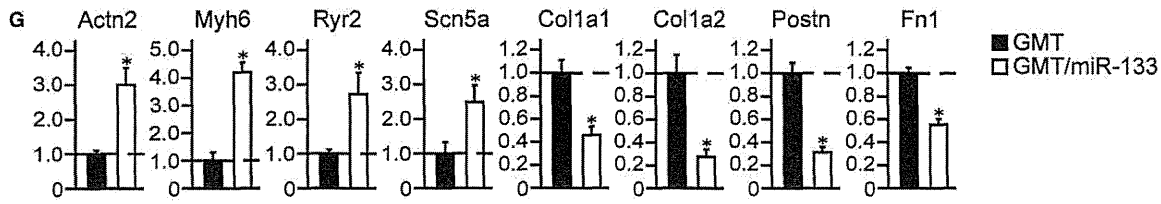

miR-133 expression was induced by GMT transduction in MEFs and further upregulated by miR-133 overexpression (Fig 4D). Inversely, the mRNA expression of *Snai1* was high in MEFs, significantly downregulated by GMT and further reduced by 60% with the addition of miR-133 to GMT, consistent with the array data (Figs 4E and 3F). Western blot analyses also demonstrated that Snai1 protein expression was strongly downregulated in MEFs by transduction with miR-133 alone or GMT/miR-133 (Fig 4F). These results

© 2014 The Authors

Figure 3. MiR-133 silences fibroblast signatures and activates cardiac programs.

A Heat-map image of microarray data illustrating the global gene expression pattern of MEFs, iCMs, and hearts. The iCMs were sorted as αMHC-GFP$^+$ cells after 3 (D3), 7 (D7), and 18 (D18) days of GMT or GMT/miR-133 transduction. Differentially expressed genes between MEFs and hearts are shown (n = 1).

B Differentially expressed genes between GMT-iCMs and GMT/miR-iCMs are shown (n = 1). See also Supplementaray Table S1.

C, D GO analyses of the upregulated (C) and downregulated (D) genes in GMT/miR-iCMs at all stages. Top 10 GO categories are shown. Cardiac (C) and fibroblast-related (D) GO terms are shown in red.

E The upregulated and downregulated genes in GMT/miR-iCMs at day 3 were analyzed by scatter plots.

F The relative mRNA expression of cardiomyocyte, fibroblast, and epithelial cell genes in D7 GMT/miR-iCMs compared to D7 GMT-iCMs by microarray.

G The relative mRNA expression of D7 GMT/miR-iCMs compared to D7 GMT-iCMs was determined by qRT-PCR (n = 3).

Data information: Data were normalized by the values of GMT-iCMs. All data are presented as means ± SEM (G). *P < 0.05, **P < 0.01 versus relevant control.

suggested that miR-133 directly targets Snai1, resulting in reduced expression of this protein during reprogramming.

Next, to investigate the possible contribution of Snai1 during cardiac reprogramming, we suppressed Snai1 expression with siRNA in GMT-transduced MEFs (Fig 4G). qRT-PCR at day 7 of transduction demonstrated that knockdown of Snai1 in the presence of GMT strongly downregulated expression of multiple fibroblast genes, including *Fn1*, *Postn*, and *Snai2*, to levels comparable with those affected by GMT/miR-133 (Fig 4H). Intriguingly, inhibition of Snai1 concomitantly upregulated a panel of cardiac genes related to different functions, such as sarcomere structures (*Actn2*, *Ttn*), gap junctions (*Gja1*), hormones (*Nppa*), and ion channels (*Ryr2* and *Kcnd2*), in GMT-transduced cells (Fig 4H, Supplementary Fig S3A). FACS analyses demonstrated that knockdown of Snai1 significantly increased the induction of α-MHC-GFP$^+$ cells and cTnT$^+$ cells from MEFs in combination with GMT, but not with GMT/miR-133 (Fig 4I and J, Supplementary Fig S3B). Immunostaining for cardiac markers, including α-actinin, cTnT, and ANP, demonstrated that Snai1 suppression increased cardiac protein expression in combination with GMT after 4 weeks (Fig 4K–M, Supplementary Fig S3C). Snai1 suppression significantly increased spontaneous Ca^{2+} oscillations and cell contractions in GMT-transduced cells, although not to the levels seen with miR-133 overexpression (Fig 4N, Supplementary Fig S3D, Supplementary Movie S4). These results suggested that suppression of Snai1 reduced fibroblast profiles and concomitantly promoted cardiac induction in GMT-transduced fibroblasts, which recapitulated the effects of miR-133 overexpression.

Overexpression of Snai1 maintains fibroblast signatures and disrupts cardiac reprogramming in GMT/miR-133-transduced MEFs

We next asked whether suppression of Snai1 is a consequence of or is required for cardiac reprogramming induced with GMT/miR-133. To address this, we restored Snai1 expression in GMT/miR-133-transduced MEFs by overexpression of Snai1 cDNA without the 3′UTR and investigated whether Snai1 restoration could counteract the effects of miR-133-mediated cardiac reprogramming (Fig 5A). Microarray analyses revealed that among 46 genes upregulated by GMT/miR-133 (Fig 3B), 39 were suppressed by Snai1 overexpression. In contrast, 105 out of 129 genes downregulated by miR-133 addition (Fig 3B) were upregulated by Snai1 restoration, suggesting most portions of the transcriptional changes effected by miR-133 were mediated via Snai1 suppression (Fig 5B). The genes upregulated and downregulated by Snai1 overexpression were identified as fibroblast- and cardiac-related genes, respectively, and qRT-PCR analyses confirmed the array data (Fig 5C, Supplementary Fig S3E and F). These results suggest that Snai1 repression is critical for silencing fibroblast programs and activating the cardiac phenotype in MEFs induced with GMT/miR-133. Snai1 overexpression also inhibited both the induction of α-MHC-GFP and cTnT expression in GMT/miR-133-transduced fibroblasts, as shown by FACS analyses (Fig 5D and E), and the expression of endogenous cardiac proteins, α-actinin, cTnT, and ANP, in GMT/miR-133-transduced cells at 4 weeks, as revealed by immunocytochemistry (Fig 5F–H, Supplementary Fig S3G). Consistent with this, constitutive expression of Snai1 strongly suppressed spontaneous Ca^{2+} oscillations in GMT/miR-133-transduced cells and inhibited generation of beating iCMs at 4 weeks, overriding the positive effects of miR-133 (Fig 5I). These results suggested that downregulation of Snai1 is critical for suppressing fibroblast profiles and cardiac reprogramming in MEFs induced with GMT/miR-133.

MiR-133-induced Snai1 suppression is critical for cardiac reprogramming in adult mouse cardiac fibroblasts

We next investigated whether the miR-133-mediated suppression of Snai1 also plays critical roles in cardiac reprogramming in adult mouse CFs. Similar to the MEF cultures, we did not detect contamination of cardiomyocytes in adult CF cultures derived from α-MHC-GFP mice. Transfection of miR-133 alone did not induce cardiac reprogramming in adult CFs either with or without the JAK inhibitor (Supplementary Fig S3H). We then introduced miR-133 with GMT and found significantly increased induction of α-MHC-GFP$^+$ and cTnT$^+$ cells from adult CFs by FACS at 1 week (Fig 6A and B). qRT-PCR demonstrated that miR-133 upregulated multiple cardiac genes and concomitantly downregulated fibroblast gene expression in adult CFs in combination with GMT (Fig 6C). Immunocytochemistry and Ca^{2+} imaging also showed that addition of miR-133 to GMT promoted cardiac induction from adult CFs (Fig 6D–G, Supplementary Movie S5). These results suggested that miR-133 promotes cardiac reprogramming in adult CFs, but with lower reprogramming efficiency compared to that in MEFs.

Next, we analyzed the link between miR-133 and Snai1 during reprogramming in adult CFs. The mRNA expression of *Snai1* was high in adult CFs, downregulated by GMT, and further reduced by 50% with the addition of miR-133 to GMT, which was inversely correlated with the expression of miR-133 (Fig 6H). qRT-PCR demonstrated that knockdown of Snai1 upregulated a panel of cardiac genes related to multiple functions and repressed fibroblast genes in GMT-transduced adult CFs (Fig 6I). Immunostaining revealed that inhibition of Snai1 increased the induction of α-MHC-GFP$^+$ cells and α-actinin$^+$ cells from adult CFs in combination with GMT (Fig 6J and K). These results suggested that suppressing Snai1

© 2014 The Authors

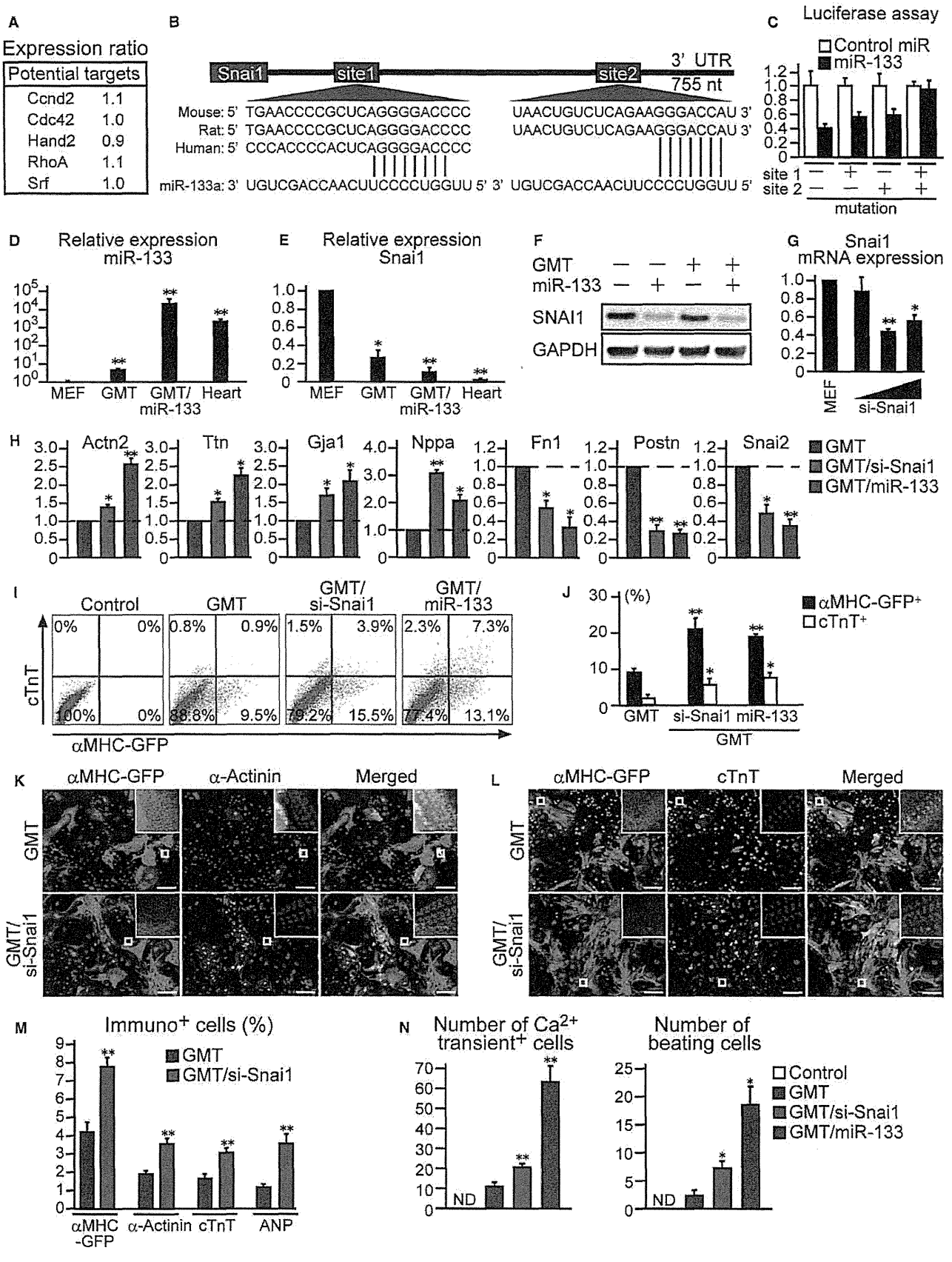

© 2014 The Authors

Figure 4. Repression of Snai1 silences fibroblast profile and promotes cardiac reprogramming.

A The relative mRNA expression of potential direct targets of miR-133 in D7 GMT/miR-iCMs compared to D7 GMT-iCMs by microarray.
B Snai1 3′UTR contains two predicted miR-133a binding sites. Both are conserved among species, shown in red.
C MiR-133a directly repressed WT Snai1 3′UTR in luciferase assay, and the repression was abolished when both of binding sites were mutated (n = 3).
D Relative miR-133a expression in MEFs, GMT-iCMs, GMT/miR133-iCMs, and hearts (n = 3).
E Relative mRNA expression of Snai1 in MEFs, GMT-iCMs, GMT/miR133-iCMs, and hearts (n = 3).
F Western blot analyses for Snai1 expression in MEFs, MEFs transfected with miR-133 alone, and MEFs transduced with GMT and GMT/miR-133.
G Relative mRNA expression of Snai1 in MEFs and MEFs transfected with siRNA against Snai1 (5, 15, 100 nM) (n = 3).
H Relative mRNA expression of cardiac (*Actn2*, *Ttn*, *Gja1*, *Nppa*) and fibroblast genes (*Fn1*, *Postn*, *Snai2*) in MEFs transduced with GMT, GMT/si-Snai1, or GMT/miR-133 (n = 3). See also Supplementary Fig S3A.
I, J FACS analyses for αMHC-GFP$^+$ and cTnT$^+$ cells 1 week after GMT transduction with si-Snai1 or miR-133 transfection. Quantitative data are shown in (J) (n = 3).
K–M Immunocytochemisty for αMHC-GFP, α-actinin, cTnT, and DAPI. Snai1 suppression increased cardiac protein expression in GMT-transduced cells (M, n = 5). See also Supplementary Fig S3C.
N Total number of Ca^{2+} oscillation$^+$ cells in 10 randomly selected fields per well is shown (the left panel, n = 8). Spontaneously beating cells were counted in each well after 4 weeks of infection (the right panel, n = 3). See also Supplementary Fig S3D and Movie S4.

Data information: All data are presented as means ± SEM. *P < 0.05, **P < 0.01 versus relevant control. Scale bars, 100 μm.

could in turn suppress fibroblast programs and promote cardiac induction in adult CFs. We then also overexpressed the Snai1 cDNA without 3′UTR in GMT/miR-133-transduced adult CFs and found reduced α-MHC-GFP$^+$ and cTnT$^+$ cells, as measured by FACS (Fig 6A and B). qRT-PCR revealed downregulated expression of cardiac genes and upregulated expression of multiple fibroblast genes by Snai1 overexpression, suggesting that Snai1 repression is critical for silencing fibroblast signatures and inducing cardiac reprogramming in adult CFs (Fig 6C). Immunocytochemistry and functional studies also revealed that Snai1 overexpression strongly inhibited cardiac reprogramming in GMT/miR-133-transduced adult CFs (Fig 6D–F).

MiR-133-mediated Snai1 repression is also critical in human cardiac reprogramming

We next tested whether miR-133-mediated Snai1 suppression also plays important roles in human cardiac reprogramming using HCFs. Transfection of miR-133 alone or 4miRs with or without JAKI-1 did not induce cardiac reprogramming (Supplementary Fig S4A). In contrast, using new lentiviral vectors to transduce the genes efficiently into HCFs (Supplementary Fig S4B), we demonstrated that transduction of lentiviral GMTMM induced cTnT$^+$ and α-actinin$^+$ cells in 2–8% of HCFs (Fig 7A and B, Supplementary Fig S4C). The induction rate increased to 23–27% of HCFs with addition of miR-133 to GMTMM (Fig 7A and B, Supplementary Fig S4C). Microarray analyses further revealed that GMTMM or GMTMM/miR-133 transduction upregulated 1,270 cardiac-enriched genes and downregulated 1,111 fibroblast-related genes in HCFs, suggesting global transcriptional changes toward cardiac fate induced by the reprogramming factors (Fig 7C). Differential gene expression analyses between GMTMM-HCFs and GMTMM/miR-133-HCFs showed that addition of miR-133 upregulated 399 genes and downregulated 264 genes (Fig 7D). GO term analyses associated the upregulated genes with cardiac function and the downregulated genes with fibroblast signatures, suggesting that miR-133 promotes cardiac reprogramming in HCFs (Fig 7E). Snai1 mRNA expression was suppressed by GMTMM and further reduced by 40% with GMTMM/miR-133 in human cardiac reprogramming (Fig 7F). Microarray analyses demonstrated that the transcriptional changes effected by miR-133 were largely counteracted by Snai1 overexpression, suggesting the miR-133-induced cardiac reprogramming was mainly mediated through Snai1 suppression (Fig 7D and G). Consistent with this, qRT-PCR, FACS analyses, and immunocytochemistry revealed that Snai1 overexpression inhibited GMTMM/miR-133-mediated cardiac induction (Fig 7A, B, H, I and J, Supplementary Fig S4D and E), whereas Snail knockdown increased the induction of cardiac genes in combination with GMTMM as measured by qRT-PCR (Supplementary Fig S4F). FACS analyses and immunostaining also demonstrated that knockdown of Snai1 significantly increased expression of α-actinin$^+$ cells in HCFs in combination with GMTMM, suggesting that suppressing Snai1 expression promotes cardiac induction (Supplementary Fig S4G–I). Taken together, these results suggest that miR-133-mediated Snai1 suppression is also crucial for human cardiac reprogramming.

Discussion

Direct reprogramming is characterized as a process that progressively activates the target cell program and concomitantly suppresses the starting-cell profile without passing through a stem cell state by overexpression of lineage-specific transcription factors or miRNAs. In this study, we demonstrated that overexpression of miR-133 in the presence of these transcription factors promoted cardiac reprogramming in mouse and human, partly by suppressing Snai1, a master regulator of EMT, and silencing the fibroblast program.

The miR-133 family comprises three miRNAs: miR-133a-1, miR-133a-2, and miR-133b. MiR-133a-1 and miR-133a-2 have identical sequences and are expressed in cardiac and skeletal muscles. Indeed, mice lacking both miR-133a-1 and miR-133a-2 undergo embryonic or neonatal death due to heart defects, suggesting critical roles of miR-133a in cardiogenesis (Liu *et al*, 2008). Consistent with this, addition of miR-133a to cardiac reprogramming factors increased cardiac reporter and gene expression, shifted the global gene expression profile of the iCMs toward a cardiac fate, and generated more functional iCMs in direct reprogramming.

Our findings support that combining lineage-specific transcription factors and miRNAs provides a powerful approach to improve direct conversion of fibroblasts into another lineage. Yoo *et al* (2011) reported that a combination of neural-specific miRNAs, miR-9/9*, and miR-124, and neurogenic transcription factors directly reprogrammed human fibroblasts into functional neuronal cells (Yoo *et al*, 2011). Recently, Nam *et al* (2013) reported that addition of miR-1 and miR-133 to Gata4, Hand2, Myocd, and Tbx5 promoted

© 2014 The Authors

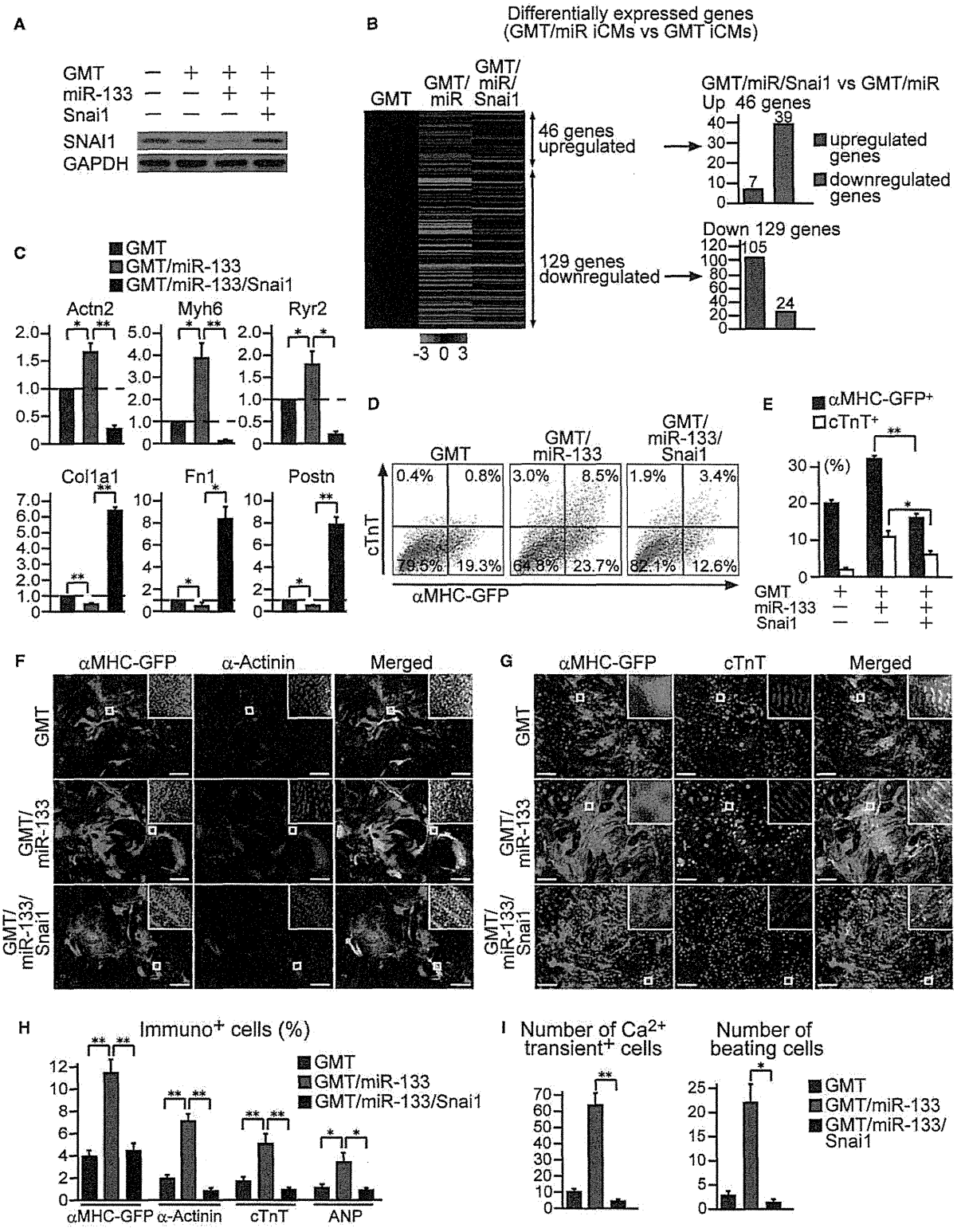

cardiac reprogramming in human fibroblasts (Nam *et al*, 2013). However, the mechanistic basis underlying direct reprogramming by the transcription factor/miRNA combinations was not established in these previous studies. Moreover, the molecular mechanisms and importance of suppressing fibroblast signatures during direct reprogramming remained largely unknown.

In the present study, we found that miR-133 suppressed a large set of fibroblast genes and concomitantly activated cardiac gene

 © 2014 The Authors

Figure 5. Overexpression of Snai1 inhibits cardiac reprogramming.

A Western blot analyses for Snai1 expression in MEFs and MEFs transduced with GMT, GMT/miR-133, and GMT/miR-133 with Snai1 overexpression.

B Heat-map image of microarray data for GMT-, GMT/miR-, and GMT/miR/Snai1-iCMs sorted as αMHC-GFP$^+$ cells after 1 week of transduction (left panel, n = 1). Differentially expressed genes between GMT-iCMs and GMT/miR-iCMs are shown (see also Fig 3B). Thirty-nine genes out of 46 upregulated genes were suppressed by Snai1 overexpression, while 105 genes out of 129 downregulated genes were increased with Snai1 transduction (right panel).

C The relative mRNA expression of D7 GMT/miR-iCMs compared to D7 GMT-iCMs was determined by qRT-PCR (n = 3). Relative mRNA expression of cardiac (*Actn2*, *Myh6*, *Ryr2*) and fibroblast genes (*Col1a1*, *Fn1*, *Postn*) in MEFs transduced with GMT and GMT/miR-133 with or without Snai1 overexpression (n = 3).

D, E FACS analyses for αMHC-GFP$^+$ and cTnT$^+$ cells 1 week after GMT and GMT/miR-133 transduction with or without Snai1 overexpression. Quantitative data are shown in (E) (n = 3).

F–H Immunocytochemisty for αMHC-GFP, α-actinin, cTnT, and DAPI. Snai1 overexpression suppressed cardiac protein expression in GMT/miR-133-transduced cells (H, n = 5).

I Numbers of Ca^{2+} oscillation$^+$ cells in 10 randomly selected fields per well are shown (left panel, n = 8). Number of spontaneously beating cells in each well after 4 weeks of infection (right panel, n = 3).

Data information: All data are presented as means ± SEM. $^*P < 0.05$, $^{**}P < 0.01$ versus relevant control. Scale bars, 100 μm.

programs during cardiac reprogramming when used in combination with GMT or GMTMM. Among many predicted targets of miR-133, we identified Snai1 as a novel direct target of the miRNA and demonstrated that Snai1 repression silences fibroblast programs and promotes cardiac reprogramming, recapitulating the effects of miR-133 overexpression. In contrast, overexpression of Snai1 inhibited suppression of fibroblast genes and activation of cardiac programming induced with GMT/miR-133. Thus, silencing fibroblast signatures, mediated by miR-133/Snai1, could be a key molecular roadblock during direct cardiac reprogramming. Intriguingly, this process is similar to the MET, a critical step during the reprogramming of fibroblasts into iPSCs by the Yamanaka factors (Li *et al*, 2010; Samavarchi-Tehrani *et al*, 2010). During iPSC generation, Oct4 and Sox2 suppress Snai1, while Klf4 induces epithelial genes including E-cadherin (Li *et al*, 2010). Snai1 downregulation and E-cadherin upregulation cooperatively suppress EMT signals and activate an epithelial program, leading to MET and iPSC generation. Similar to our findings, blocking MET by overexpression of Snai1 or addition of a Snai1 activator (transforming growth factor β) impaired iPSC generation, whereas inducing MET by addition of transforming growth factor β inhibitors promoted iPSC induction (Li *et al*, 2010; Samavarchi-Tehrani *et al*, 2010). Thus, it is conceivable that silencing fibroblast signatures by repressing Snai1 might be a common pathway in the early phase of reprogramming from fibroblasts to another lineage and that manipulation of this pathway could be a new target to enhance direct reprogramming in general. To our knowledge, this is the first study demonstrating a molecular mechanism of direct cardiac reprogramming.

While we found that the miR-133/Snai1 pathway is critical for cardiac reprogramming, the iCM population was heterogeneous and most of the cells remained as partially reprogrammed cardiac cells in culture (Supplementary Table S2). Moreover, the reprogramming efficiency of adult CFs was low compared with MEFs in this study and our previous data using neonatal CFs (Ieda *et al*, 2010). Differences between mouse lines used and transcriptional and epigenetic differences between fibroblasts might have contributed to the lower reprogramming efficiency in adult CFs. Because miR-133 has numerous predicted targets, and knockdown of Snai1 increased cardiac induction, but not to the level observed with miR-133 overexpression, some additional pathways might be involved in miR-133-mediated cardiac reprogramming (Liu & Olson, 2010). Nevertheless, given that the *in vivo* environment might be more permissive than culture dishes for reprogramming, GMT/miR-133 transduction or Snai1 knockdown with GMT *in vivo* might be sufficient to repair damaged hearts (Qian *et al*, 2012; Song *et al*, 2012). Further *in vitro* and *in vivo* studies are thus needed to progress our understanding of molecular mechanisms underlying cardiac reprogramming and apply this new technology to future regenerative therapies.

Materials and Methods

Generation of αMHC-GFP and Mesp1-GFP mice

Transgenic mice overexpressing GFP under the control of an α-MHC promoter were generated as described previously (Ieda *et al*, 2010). Mesp1-GFP mice were obtained by crossing Mesp1-Cre mice and CAG-CAT-EGFP reporter mice (Saga *et al*, 1999; Kawamoto *et al*, 2000). The Keio University Ethics Committee for Animal Experiments approved all experiments in this study.

Quantitative RT–PCR

Total RNA was isolated from cells, and qRT-PCR was performed on a StepOnePlus™ (Applied Biosystems) with TaqMan probes (Applied Biosystems). TaqMan probes: *Actc1* (Mm01333821_m1, Hs00606316_m1), *Myh6* (Mm00440354_m1, Hs00411908_m1), *Ryr2* (Mm00465877_m1, Hs00892842_m1), *Gja1* (Mm00439105_m1), *Nppa* (Mm01255747_g1, Hs00383230_g1), *Actn2* (Mm00473657_m1, Hs00153809_m1), *Kcnd2* (Mm0116732_m1), *Slc8a1* (Mm01232254_m1, Hs01062258_m1), *Scn5a* (Mm00451971_m1), *Tnni3* (Mm00437164_m1), *Tnnt2* (Hs00165960_m1), *Ttn* (Mm00621005_m1, Hs00399225_m1), *Myl2* (Mm00440384_m1, Hs00166405_m1), *Myl7* (Mm00491655_m1), *Hcn4* (Mm01176086_m1), *isl1* (Mm00517585_m1), *Col1a1* (Mm00801666_g1, Hs00164004_m1), *Col1a2* (Mm00483888_m1), *Col3a1* (Mm01254476_m1), *Col5a2* (Mm00483675_m1), *Fn1* (Mm01256744_m1, Hs00365052_m1), *Snai1* (Mm00441533_g1, Hs00195591_m1), *Snai2* (Mm00441531_m1), *Ddr2* (Mm0000445615_m1), *Postn* (Mm00450111_m1, Hs00170815_m1), *Hsa-miR-133a* (1102119-Q). mRNA levels were normalized by comparison to *Gapdh* (Mm99999915_g1, Hs02758991_g1). miRNA levels were normalized by comparison to *Rnu6b* (0811824-H) snRNA.

Molecular cloning, retroviral infection, lentiviral infection, and miRNA mimics transfection

To construct the pMXs retroviral vectors, we amplified the coding regions of GFP, Gata4, Mef2c, Tbx5, and Snai1 by PCR and

© 2014 The Authors

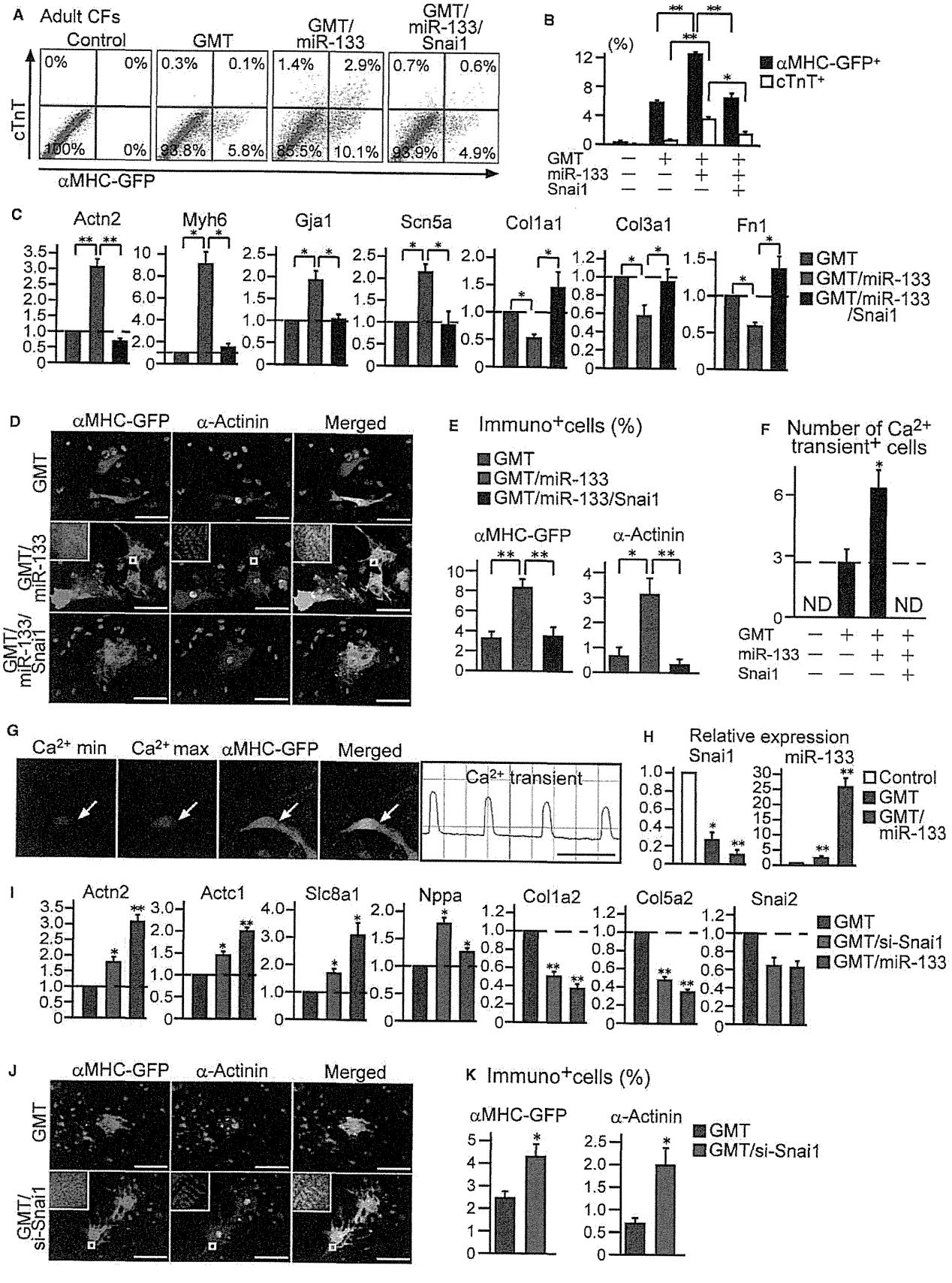

© 2014 The Authors

Figure 6. MiR-133-mediated Snai1 repression is critical for cardiac reprogramming in adult cardiac fibroblasts.

A, B FACS analyses for αMHC-GFP$^+$ and cTnT$^+$ cells in adult CFs 1 week after GMT and GMT/miR-133 transduction with or without Snai1 overexpression. Quantitative data are shown in (B) (n = 3).

C Relative mRNA expression of cardiac (*Actn2*, *Myh6*, *Gja1*, *Scn5a*) and fibroblast genes (*Col1a1*, *Col3a1*, *Fn1*) in adult CFs transduced with GMT and GMT/miR-133 with or without Snai1 overexpression (n = 3).

D, E Immunocytochemisty for αMHC-GFP and α-actinin with DAPI staining in GMT, GMT/miR-133, or GMT/miR-133/Snai1-transduced adult CFs 4 weeks after transduction. High-magnification views in insets show sarcomeric organization. Quantitative data are shown in (E) (n = 5).

F, G Total number of Ca^{2+} oscillation$^+$ cells in 10 randomly selected fields per well is shown in (F) (n = 3). Spontaneous Ca^{2+} oscillations observed in adult CF-derived GMT/miR-133-iCMs (arrows in G), corresponding to Supplementary Movie S5. The Rhod-3 images and intensity trace are shown in (G).

H Relative Snai1 mRNA and miR-133a expression in adult CFs, GMT-iCMs, and GMT/miR133-iCMs (n = 3).

I Relative mRNA expression of cardiac (*Actn2*, *Actc1*, *Slc8a1*, *Nppa*) and fibroblast genes (*Col1a2*, *Col5a2*, *Snai2*) in adult CFs transduced with GMT, GMT/si-Snai1, or GMT/miR-133 (n = 3).

J, K Immunocytochemisty for αMHC-GFP and α-actinin in GMT or GMT/si-Snai1 transduced adult CFs 4 weeks after transduction. High-magnification views in insets show sarcomeric organization. Quantitative data are shown in (K) (n = 5).

Data information: All data are presented as means ± SEM. $^*P < 0.05$, $^{**}P < 0.01$ versus relevant control. Scale bars, 100 μm.

subcloned them into respective pMXs vectors for transfection into Plat-E cells using Fugene 6 (Roche) to generate retroviruses (Ieda *et al*, 2010). We generated lentiviral vectors by subcloning human Gata4, Mef2c, Tbx5, Mesp1, Myocd, and Snai1 (HuPEX, AIST) into the CSII-CMV-RfA plasmid (RIKEN BRC) using the Gateway system (Invitrogen). To generate the lentiviruses, we transfected the vectors into HEK293 cells with pCAG-HIVgp and pCMV-VSV-G-RSV-Rev plasmids (RIKEN BRC) using Lipofectamine 2000 (Invitrogen). The CSII-CMV-Venus vector was used to determine transduction efficiency. Virus-containing supernatants were collected after 48 h and used for transduction. Synthetic mimics of mature miRNAs (Thermo Scientific) and the siRNA pool (Thermo Scientific) were transfected simultaneously into cells with Lipofectamine 2000 (Invitrogen). Synthetic mimics of mature miRNAs and siRNA pool: miRIDIAN microRNA Mouse mmu-miR-1-Mimic (C-310376-07-0020), miRIDIAN microRNA Mouse mmu-miR-133a-Mimic (C-310407-07-0020), miRIDIAN microRNA Mouse mmu-miR-208a-3p-Mimic (C-310501-05-0020), miRIDIAN microRNA Mouse mmu-miR-499-Mimic (C-310727-01-0020), miRIDIAN microRNA Mimic Negative Control #2 (CN-002000-01-05), siGENOME Mouse Snai1 siRNA - SMARTpool (M-062765-00-0020), siGENOME Human Snai1 siRNA - SMARTpool (M-010847-00-0020). After 24 h, the medium was replaced with D-MEM (high glucose) with L-Glutamate and Phenol Red (Wako, 044-29765)/Medium199 with Earle's Salts, L-Glutamate and 22 g/l Sodium Bicarbonate (Gibco, 11150-059)/10% Hyclone Characterized FBS (Thermo Scientific, SV30014.03) medium and changed every 2–3 days. JAK inhibitor I (1 nM, EMD Biosciences) treatment was initiated 2 days after transfection and continued daily for 7 days.

Cell culture

For MEF isolation, embryos isolated from 12.5-day pregnant mice were washed with PBS, and the head and visceral tissues were carefully removed. The remaining parts of the embryos were washed in fresh PBS, minced using a pair of scissors, transferred into a 0.25 mM trypsin/1 mM EDTA solution (3 ml per embryo), and incubated at 37°C for 20 min. An additional 3 ml of trypsin/EDTA solution was then added, and the mixture was further incubated at 37°C for 20 min. After trypsinization, an equal amount of medium (6 ml of DMEM containing 10% FBS per embryo) was added and pipetted up and down a few times to help tissue dissociation. After incubation of the tissue/medium mixture for 5 min at room temperature, the supernatant was transferred into a new tube and cells were collected by centrifugation and resuspended in DMEM/10% FBS (Thermo Scientific, SV30014.03) for culturing at 37°C in 5% CO_2. For isolation of mouse adult cardiac fibroblasts, αMHC-GFP TG adult mouse hearts were minced into small pieces < 1 mm^3 in size. The explants were plated on gelatin-coated dishes and cultured for 10–14 days in explant medium (IMDM with L-Glutamate and 25 mM HEPES (Gibco, 12440-053)/20% FBS). Migrated fibroblasts were harvested and filtered with 40-μm cell strainers (BD) to avoid contamination with tissue fragments. The αMHC-GFP$^-$/Thy1$^+$ CFs were FACS sorted and plated at a density of $10^4/cm^2$ for the retrovirus transduction.

Human atrial tissues were obtained from patients undergoing cardiac surgery (age 1 month to 80 year; average age, 35 year) with informed consent in conformation with the guidelines of the Keio University Ethics Committee. For isolation of human cardiac fibroblasts, human hearts were minced into small pieces < 1 mm^3 in size. The explants were plated on gelatin-coated dishes and cultured for 14 days in the explant medium. Migrated fibroblasts were harvested, filtered with 40-μm cell strainers (BD), and plated at a density of $5 \times 10^3/cm^2$ for the virus transduction. For all experiments, we used fibroblasts of early passage number (P1-3). The Keio Center for Clinical Research approved all of the human experiments in this study (20100131).

FACS analyses and sorting

For GFP expression analyses, cells were harvested from culture dishes and analyzed on a FACSCalibur (BD Biosciences) with FlowJo software. For αMHC-GFP/cTnT expression, cells were fixed with 4% PFA for 15 min, permealized with saponin, and stained with anti-cTnT and anti-GFP antibodies, followed by secondary antibodies conjugated with Alexa 488 and 647, respectively. For α-actinin or cTnT expression, cells were stained with anti-α-actinin or cTnT antibody, followed by secondary antibody conjugated with Alexa 647. For iCM sorting, cells were sorted as αMHC-GFP$^+$ cells, and for Mesp1-GFP$^-$/Thy1$^+$ cell sorting, cells were incubated with APC-conjugated anti-Thy1 antibody (eBioscience) and sorted by FACS Aria.

Immunocytochemistry

Cells were fixed in 4% paraformaldehyde for 15 min at room temperature, blocked by 5% serum, and incubated with primary antibodies against sarcomeric α-actinin (Sigma Aldrich), vimentin

© 2014 The Authors

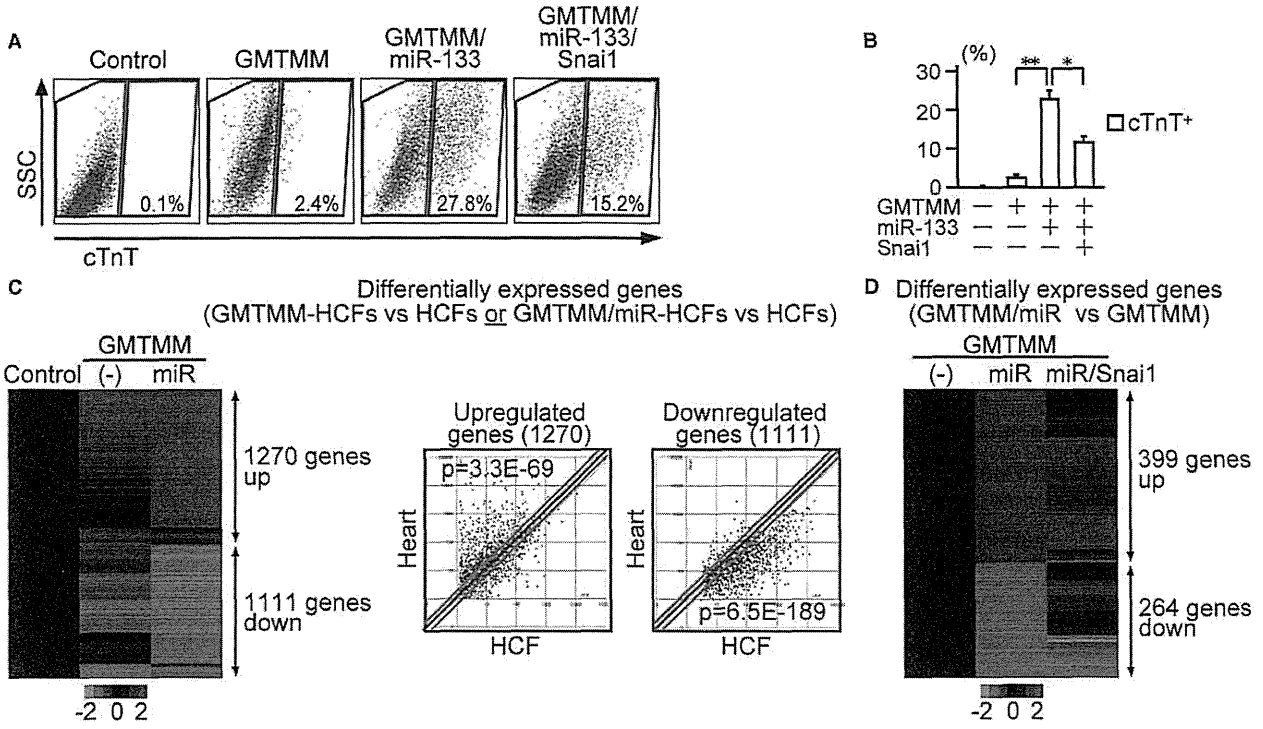

E GO categories enriched in GMTMM/miR-HCFs

Upregulated genes (399)

GO term	Genes	Size	p-value
Muscle filament sliding	10	37	1.0E-11
Cardiac muscle contraction	6	21	1.1E-7
Muscle organ development	10	94	1.5E-7
Cardiac muscle morphogenesis	5	25	9.0E-6
Heart development	10	147	9.2E-6

Downregulated genes (264)

GO term	Genes	Size	p-value
Collagen biosynthetic process	2	6	6.8E-4
Protein heterotrimerization	2	6	6.8E-4
Elastic fiber assembly	2	6	6.8E-4
Wound healing	4	60	7.5E-4
Cell adhesion	11	553	4.9E-2

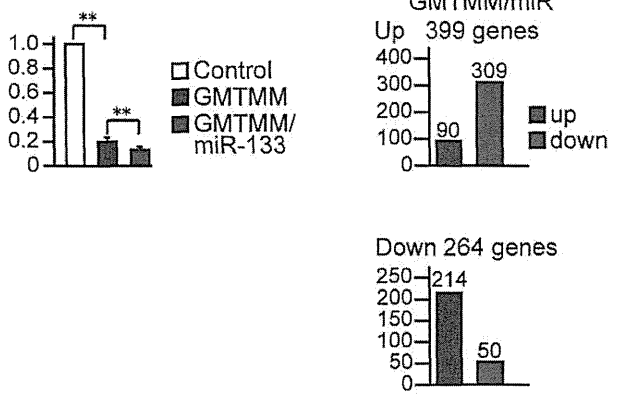

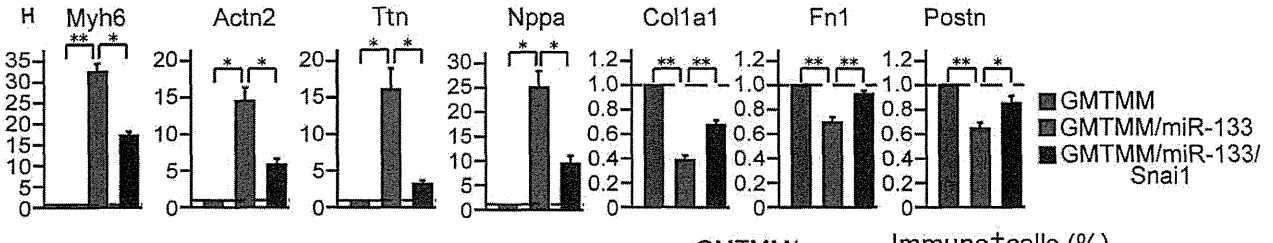

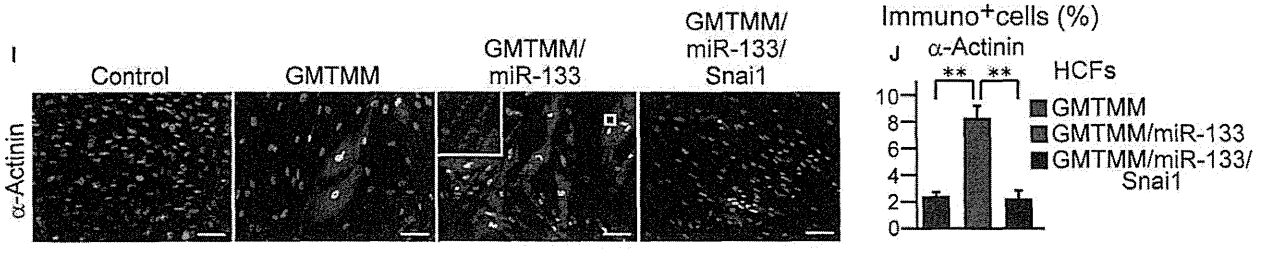

© 2014 The Authors

Figure 7. MiR-133/Snai1 pathway is critical for human cardiac reprogramming.

A, B FACS analyses for cTnT$^+$ cells in HCFs 1 week after GMTMM, GMTMM/miR-133, and GMTMM/miR-133/Snai1 transduction. Quantitative data are shown in (B) (n = 4).

C Heat-map image of microarray data illustrating the global gene expression pattern of HCFs, GMTMM-HCFs, and GMTMM/miR-133-HCFs after 1 week of transduction (n = 1, left panel). The differentially expressed genes between GMTMM- or GMTMM/miR-133-HCFs and HCFs are shown. Cardiac genes were upregulated and fibroblast genes were downregulated by transduction of the reprogramming factors, as shown in the scatter plot analyses (right panel).

D 399 genes were upregulated and 264 genes were downregulated by the addition of miR-133 to GMTMM.

E GO term analyses of the upregulated and downregulated genes, shown in (D). Cardiac- and fibroblast-related GO terms are shown.

F The mRNA expression of Snai1 in HCFs, GMTMM-HCFs, and GMTMM/miR-133-HCFs (n = 3).

G Snai1 restoration counteracted the effects of miR-133. 309 out of 399 upregulated genes were suppressed by Snai1 overexpression, while 214 out of 264 downregulated genes were increased with Snai1. See also Fig 7D.

H Relative mRNA expression of cardiac (*Myh6, Actn2, Ttn, Nppa*) and fibroblast genes (*Col1a1, Fn1, Postn*) in GMTMM-, GMTMM/miR-133-, and GMTMM/miR-133/Snai1-HCFs after 1 week of transduction (n = 3).

I, J Immunocytochemisty for α-actinin and DAPI. Snai1 overexpression suppressed cardiac protein expression in GMTMM/miR-133-transduced HCFs (J, n = 10). High-magnification view in inset shows sarcomeric organization.

Data information: All data are presented as means ± SEM. $^*P < 0.05$, $^{**}P < 0.01$ versus relevant control. Scale bars, 100 μm.

(Progen), Collagen 1 (Millipore), GFP (Invitrogen), cTnT (Thermo Scientific), ANP (Millipore), Myl7 (Synaptic Systems), or Nkx2.5 (Santa Cruz), and subsequently with secondary antibodies conjugated with Alexa 488 or 546 (Molecular Probes), followed by DAPI counterstaining (Invitrogen). The percentage of cells immunopositive for GFP, α-actinin, cTnT, and ANP were counted in six randomly selected fields per well in three independent experiments, and 500–1,000 cells were counted in total. The measurements and calculations were made in a blinded manner.

EdU labeling assay

For the experiments assessing cell proliferation, 10 μM EdU was added to the culture medium after 2 weeks of transduction and maintained throughout the culture for a further 2 weeks. Cells were fixed with 4% paraformaldehyde for 15 min, permeabilized, incubated with anti-cTnT antibody followed by secondary antibody conjugated with Alexa 546 (for immunocytochemistry) or 647 (for FACS), and then incubated with the EdU reaction cocktail following the manufacturer's instructions (Invitrogen).

Ca^{2+} imaging and counting beating cells

Ca^{2+} imaging was performed according to the standard protocol. Briefly, cells were labeled with Rhod-3 (Invitrogen) for 1 h at room temperature, washed, and incubated for an additional 1 h to allow de-esterification of the dye. Rhod-3 labeled cells were analyzed at 37°C by LSM 510 META confocal microscopy (Carl Zeiss). Imaging of the Ca^{2+} oscillations was possible for only a short time due to the increasing background fluorescence from the medium, and thus, the measurements were taken within 30 min after changing to the Tyrode's buffer. The Ca^{2+} oscillation$^+$ cells were counted in 10 randomly selected fields per well in at least three independent experiments, and a minimum of 1,000 cells were counted in total. The total number of Ca^{2+} oscillation$^+$ cells in 10 randomly selected fields per well is shown.

For counting beating cells, we seeded 50,000 fibroblasts per well on 12-well plates, performed cell transductions, and then monitored cell contraction. The number of spontaneously contracting cells was manually counted in each well in at least three independent experiments. The number of beating cells per well is shown. The measurements and calculations were made in a blinded manner.

Western blotting

Lysates were prepared by homogenization of cells in RIPA buffer and run on SDS–PAGE to separate proteins prior to the immunoblot analyses. After transfer to nitrocellulose membranes, immunodetection was performed with antibodies to Snai1 (Abcam) and Gapdh (Cell Signaling Technology), followed by the appropriate HRP-conjugated secondary antibodies (Cell Signaling Technology). The antibody-bound proteins were visualized by chemiluminescence detection (ECL, Amersham).

Dual-luciferase reporter assay

For construction of the Snai1 3′UTR reporter, the CMV promoter was subcloned into the promoterless pGL3-Basic vector (Promega) upstream of the luciferase gene. A 755-bp Snai1 3′UTR fragment containing miR-133a-binding sites was amplified by PCR and subcloned into the modified pGL3-Basic vector. The activities of firefly luciferase and renilla luciferase in the control vector were determined by the dual-luciferase reporter assay (Promega). Mutations of the AGGGGACCA miR-133a seed binding sequence were constructed through PCR-based mutagenesis (Stratagene). The miRNA target prediction program (http://cbio.mskcc.org/cgi-bin/mirnaviewer/mirnaviewer.pl) was used to identify putative targets.

Gene microarray analyses

Mouse genome-wide gene expression analyses were performed using 3D-Gene Mouse Oligo chip 25k (Toray Industries Inc.). For efficient hybridization, this microarray is three-dimensional and is constructed with a well as the space between the probes and cylinder stems with 70-mer oligonucleotide probes on the top. RNA was extracted from MEFs, GMT-, GMT/miR-133-, or GMT/miR-133/Snai1-induced αMHC-GFP$^+$ cells, neonatal mouse heart tissues, HCFs, GMTMM-, GMTMM/miR-133-, GMTMM/miR-133/Snai1-transduced HCFs using ReliaPrep™ RNA Cell Miniprep System (Promega). Total RNA was labeled with Cy5 using the Amino Allyl MessageAMP II aRNA Amplification Kit (Applied Biosystems), and the hybridization was performed using the supplier's protocols (www.3d-gene.com). Hybridization signals were scanned using 3D-Gene Scanner (Toray Industries Inc.) and processed by extraction (Toray Industries Inc.). The raw data of each spot were normalized

© 2014 The Authors

by substitution with a mean intensity of the background signal determined by the combined signal intensities of all blank spots at 95% confidence intervals. Raw data intensities > 2 standard deviations (SD) of the background signal intensity were considered to be valid. Detected signals for each gene were normalized by the global normalization method. Heatmap images for differentially expressed genes (more than 2-fold or 1.5-fold difference) were processed using the Cluster 2.0 software, and the results were displayed with the TreeView program (http://rana.lbl.gov/eisen/). Scatter plot analyses were processed using Microsoft Excel. Gene ontology (GO) analysis was performed using GeneCodis. This method computes hypergeometric *P*-values for over- or under-representation of each GO term in the specified ontology for the gene set of interest. Moderated *t*-statistics and the associated *P*-values were calculated by the Welch *t*-test using Microsoft Excel. Differential gene expression was defined using the statistics/threshold combination.

Statistical analyses

Differences between groups were examined for statistical significance using Student's *t*-test or ANOVA. *P*-values of < 0.05 were regarded as significant.

Data deposition

Microarray data are deposited in GEO with accession number GSE56913.

Supplementary information for this article is available online: http://emboj.embopress.org

Acknowledgements

We are grateful to members of the Fukuda lab, S. Mikami, H. Mochizuki, and H. Miyoshi (RIKEN BRC), for discussion and reagents. M. I. was supported by research grants from JST CREST, JSPS, the Mitsubishi Foundation, Banyu Life Science, the Uehara Memorial Foundation, Senshin Medical Research Foundation, AstraZeneca, and Takeda Science Foundation, and N. M. was supported by research grants from Japan Heart Foundation Research Grant, Keio University Medical Science Fund, and Keio University Grant-in-Aid for Encouragement of Young Scientists.

Author contributions

NM and MI designed the experiments. NM, HYamak, KM, TS, TM, MI, HN, MA, RW, KI, YK, RA, HYamag, and NG carried out the experiments. NM, TN, RK, TF, STa, STo, HH, and KF analyzed the data. NM and MI wrote the paper.

Conflict of interest

The authors declare that they have no conflict of interest.

References

Addis RC, Epstein JA (2013) Induced regeneration–the progress and promise of direct reprogramming for heart repair. *Nat Med* 19: 829–836

Chen JX, Krane M, Deutsch MA, Wang L, Rav-Acha M, Gregoire S, Engels MC, Rajarajan K, Karra R, Abel ED, Wu JC, Milan D, Wu SM (2012) Inefficient reprogramming of fibroblasts into cardiomyocytes using gata4, mef2c, and tbx5. *Circ Res* 111: 50–55

Fu JD, Stone NR, Liu L, Spencer CI, Qian L, Hayashi Y, Delgado-Olguin P, Ding S, Bruneau BG, Srivastava D (2013) Direct reprogramming of human fibroblasts toward a cardiomyocyte-like state. *Stem Cell Rep* 1: 235–247

Han DW, Tapia N, Hermann A, Hemmer K, Hoing S, Arauzo-Bravo MJ, Zaehres H, Wu G, Frank S, Moritz S, Greber B, Yang JH, Lee HT, Schwamborn JC, Storch A, Scholer HR (2012) Direct reprogramming of fibroblasts into neural stem cells by defined factors. *Cell Stem Cell* 10: 465–472

Ieda M, Fu JD, Delgado-Olguin P, Vedantham V, Hayashi Y, Bruneau BG, Srivastava D (2010) Direct reprogramming of fibroblasts into functional cardiomyocytes by defined factors. *Cell* 142: 375–386

Inagawa K, Miyamoto K, Yamakawa H, Muraoka N, Sadahiro T, Umei T, Wada R, Katsumata Y, Kaneda R, Nakade K, Kurihara C, Obata Y, Miyake K, Fukuda K, Ieda M (2012) Induction of cardiomyocyte-like cells in infarct hearts by gene transfer of Gata4, Mef2c, and Tbx5. *Circ Res* 111: 1147–1156

Jayawardena TM, Egemnazarov B, Finch EA, Zhang L, Payne JA, Pandya K, Zhang Z, Rosenberg P, Mirotsou M, Dzau VJ (2012) MicroRNA-mediated in vitro and in vivo direct reprogramming of cardiac fibroblasts to cardiomyocytes. *Circ Res* 110: 1465–1473

Judson RL, Babiarz JE, Venere M, Blelloch R (2009) Embryonic stem cell-specific microRNAs promote induced pluripotency. *Nat Biotechnol* 27: 459–461

Kawamoto S, Niwa H, Tashiro F, Sano S, Kondoh G, Takeda J, Tabayashi K, Miyazaki J (2000) A novel reporter mouse strain that expresses enhanced green fluorescent protein upon Cre-mediated recombination. *FEBS Lett* 470: 263–268

Li R, Liang J, Ni S, Zhou T, Qing X, Li H, He W, Chen J, Li F, Zhuang Q, Qin B, Xu J, Li W, Yang J, Gan Y, Qin D, Feng S, Song H, Yang D, Zhang B *et al* (2010) A mesenchymal-to-epithelial transition initiates and is required for the nuclear reprogramming of mouse fibroblasts. *Cell Stem Cell* 7: 51–63

Liu N, Bezprozvannaya S, Williams AH, Qi X, Richardson JA, Bassel-Duby R, Olson EN (2008) microRNA-133a regulates cardiomyocyte proliferation and suppresses smooth muscle gene expression in the heart. *Genes Dev* 22: 3242–3254

Liu N, Olson EN (2010) MicroRNA regulatory networks in cardiovascular development. *Dev Cell* 18: 510–525

Marro S, Pang ZP, Yang N, Tsai MC, Qu K, Chang HY, Sudhof TC, Wernig M (2011) Direct lineage conversion of terminally differentiated hepatocytes to functional neurons. *Cell Stem Cell* 9: 374–382

Muraoka N, Ieda M (2014) Direct reprogramming of fibroblasts into myocytes to reverse fibrosis. *Annu Rev Physiol* 76: 21–37

Nam YJ, Song K, Luo X, Daniel E, Lambeth K, West K, Hill JA, DiMaio JM, Baker LA, Bassel-Duby R, Olson EN (2013) Reprogramming of human fibroblasts toward a cardiac fate. *Proc Natl Acad Sci USA* 110: 5588–5593

Protze S, Khattak S, Poulet C, Lindemann D, Tanaka EM, Ravens U (2012) A new approach to transcription factor screening for reprogramming of fibroblasts to cardiomyocyte-like cells. *J Mol Cell Cardiol* 53: 323–332

Qian L, Huang Y, Spencer CI, Foley A, Vedantham V, Liu L, Conway SJ, Fu JD, Srivastava D (2012) In vivo reprogramming of murine cardiac fibroblasts into induced cardiomyocytes. *Nature* 485: 593–598

Rowe RG, Li XY, Hu Y, Saunders TL, Virtanen I, Garcia de Herreros A, Becker KF, Ingvarsen S, Engelholm LH, Bommer GT, Fearon ER, Weiss SJ (2009) Mesenchymal cells reactivate Snail1 expression to drive three-dimensional invasion programs. *J Cell Biol* 184: 399–408

 © 2014 The Authors